Performance of GPCP Products Over Oceans: Evaluation Using Passive Aquatic Listeners

Zhe Li[1], Elizabeth J Thompson[2], Ali Behrangi[3], Haonan Chen[4], and Jie Yang[5]

[1]Colorado State University
[2]NOAA Earth System Research Lab
[3]University of Arizona
[4]Colorado State Universitying
[5]Applied Physics Laboratory, University of Washington

May 2, 2023

Abstract

Passive Aquatic Listeners (PALs) have been increasingly deployed to collect minute-scale surface oceanic rainfall and wind information, with a sampling area similar to the spaceborne sensor footprints. This provides an unprecedented opportunity to validate satellite precipitation products over oceans. This study evaluates the Global Precipitation Climatology Project (GPCP) daily products, including the widely-used GPCP v1.3 and the newly released GPCP v3.2, over oceans using 58 PALs as references. The study shows that the GPCP performance depends on time scale, region, and rainfall intensity. The two versions of GPCP perform similarly at multi-year and monthly scales, while GPCP v3.2 shows substantial improvements in representing rain occurrence and rain intensity at daily scale. The results also highlight the challenge of precipitation measurement over certain regions such as the tropical Northeastern Pacific and extratropical North Pacific, where both versions of the GPCP products perform similarly but exhibit noticeable differences compared to PAL observations.

Performance of GPCP Products Over Oceans: Evaluation Using Passive Aquatic Listeners

Zhe Li[1], Elizabeth J. Thompson[2], Ali Behrangi[3], Haonan Chen[1], Jie Yang[4]

[1]Department of Electrical and Computer Engineering, Colorado State University, Fort Collins, CO 80523, USA
[2]NOAA Physical Sciences Laboratory, Boulder, CO 80305, USA
[3]Department of Hydrology and Atmospheric Sciences, The University of Arizona, Tucson, AZ 85721, USA
[4]Applied Physics Laboratory, University of Washington, Seattle, WA 98105, USA

Key Points:

- Passive Aquatic Listeners (PALs) are used to validate GPCP products over global oceans.
- Newly released GPCP Version 3.2 and the previous Version 1.3 daily products are compared.
- The performance of GPCP products depends on time scale, location, and rainfall intensity.

Corresponding author: Dr. Zhe Li, zhe.li@colostate.edu

Abstract

Passive Aquatic Listeners (PALs) have been increasingly deployed to collect minute-scale surface oceanic rainfall and wind information, with a sampling area similar to the spaceborne sensor footprints. This provides an unprecedented opportunity to validate satellite precipitation products over oceans. This study evaluates the Global Precipitation Climatology Project (GPCP) daily products, including the widely-used GPCP v1.3 and the newly released GPCP v3.2, over oceans using 58 PALs as references. The study shows that the GPCP performance depends on time scale, region, and rainfall intensity. The two versions of GPCP perform similarly at multi-year and monthly scales, while GPCP v3.2 shows substantial improvements in representing rain occurrence and rain intensity at daily scale. The results also highlight the challenge of precipitation measurement over certain regions such as the tropical Northeastern Pacific and extratropical North Pacific, where both versions of the GPCP products perform similarly but exhibit noticeable differences compared to PAL observations.

Plain Language Summary

Satellites are the main instruments to quantify precipitation over the ocean, but it is difficult to check their accuracy because we do not have many rain gauges over oceans to compare with satellites. The Passive Aquatic Listener (PAL) is "the underwater phone" to listen to the sound generated when raindrops hit the sea surface. The PAL estimates rain rates based on the loudness of the sound at each frequency. This is similar to listening to the rain under a tin roof. PAL can drift with ocean currents for years, so it can collect rainfall data over a large ocean area. The Global Precipitation Climatology Project (GPCP) product is a popular long-term satellite-based precipitation data record to study climate, water cycle, and the ocean. This study uses PAL observations to evaluate the performance of GPCP's latest two versions: v1.3, and the newly released GPCP v3.2. The results show that the new product is better than the old product in estimating daily rainfall, while they are similar when estimating monthly and multi-year rainfall. We also notice that they provide similar estimates, which are both quite different from PAL observations, over the tropical Northeastern Pacific and extratropical North Pacific.

1 Introduction

Precipitation is an essential component of the global water and energy cycles. For this reason, it has long been recognized that accurate knowledge of the time, amount, and distribution of precipitation plays a fundamental role in understanding the Earth's climate system (Hartmann, 2016). As the largest reservoir of water in this system, the oceans receive over 75% of global precipitation and contribute approximately 85% of atmospheric water vapor through evaporation (Lagerloef et al., 2010). The difference between precipitation and evaporation (also known as the ocean-atmosphere freshwater flux) directly affects the upper ocean temperature, salinity, density, stability, and turbulence (Moum & Smyth, 2019; Sallée et al., 2021; O'Kane et al., 2016), This influences oceanic and atmospheric circulations and heat content, which regulate climate variability across multiple scales (Schmitt, 1995; Durack, 2015). Despite its importance, oceanic precipitation remains one of the least understood elements in the Earth's climate system due to the lack of in-situ observations over oceans (Trenberth et al., 2007; Kidd et al., 2017).

To fill this gap, satellites have played a major role to quantify oceanic precipitation. The precipitation-capable spaceborne sensors include infrared (IR), passive microwave (PMW) imagers/sounders, and radars. Since each type of sensor has its own strengths and limitations, today's satellite-based precipitation products are built upon a multi-sensor approach, which integrates the measurements from a constellation of spaceborne sensors to maximize the accuracy, coverage, and resolution of precipitation estimates on a global scale (Kidd et al., 2021). Furthermore, long-term climate records of global precipitation can only be achieved through such a multi-sensor strategy (Levizzani et al., 2018). In this regard, the Global Precipitation Climatology Project (GPCP) was developed by merging PMW/IR sensors and rain gauges (over land) to provide this information to the international community. For a long time, GPCP linked to the World Climate Research Programme (WCRP) and Global Energy and Water Experiment (GEWEX) activities (Adler et al., 2020).

GPCP was first introduced in the mid-1990s (Arkin & Xie, 1994; Huffman et al., 1997), and since then, it has undergone several iterations to improve the input data sources, merging algorithms, and resolution (Huffman et al., 2001; Adler et al., 2003; Huffman et al., 2023a). GPCP products have been widely used to study the precipitation climatology and the hydrologic cycle (e.g., Yu, 2011; Lagerloef et al., 2010). However, validating satellite-based precipitation estimates, including GPCP, over oceans remains challenging. The in-situ reference data for validation are generally limited to rain gauges, which are only available from a small number of atoll/islands sites, moored buoys, and research vessels (Bowman, 2005; Sapiano & Arkin, 2009; Pfeifroth et al., 2013; Bolvin et al., 2021). Additionally, rain gauges may provide an incomplete representation of precipitation compared to satellite data, due to the point sampling nature of gauges relative to satellite grid box estimates that are several kilometers wide (Kidd et al., 2021). To overcome data limitations at sea, several other ocean-specific precipitation instruments have emerged, such as ship-based optical disdrometers (Klepp et al., 2018), ship-based motion-stabilized radars (Rutledge et al., 2019), and the subsurface Passive Aquatic Listeners (PAL; Ma & Nystuen, 2005; Yang et al., 2015).

Different from rain gauge or ship-based sensors, PAL is an underwater acoustic sensor (hydrophone) typically mounted on drifting Argo floats (Roemmich et al., 2019), which can collect oceanic rainfall and wind information at minute-scale over a large domain. In addition, a PAL has a sampling area similar to the footprint of spaceborne sensors, making it more comparable to satellite data. Since 2010, 58 PALs have been deployed over different oceans, and their observations were recently reprocessed and made available for use (Yang et al., 2015; Bytheway et al., 2023). In this study, we leverage this newly-available oceanic rainfall dataset to validate GPCP daily products over the ocean. To our best knowledge, this work represents the most expansive validation of GPCP daily data over oceans because it uses the distributed set of in-situ observations available from the state-of-the-art multiyear PAL database.

2 Data

2.1 Passive Aquatic Listeners

PAL is an innovative acoustic sensor, a hydrophone, designed to measure rain rate and wind speed routinely over the ocean (J. A. Nystuen et al., 2015; Yang et al., 2015). It collects underwater ambient-noise time series at different frequencies and converts them into a multi-frequency (1-50 kHz) spectrum of sound pressure levels (SPL). The overall SPL can be attributed to different sources of ocean ambient sound such as raindrops, surface wind, wave breaking, marine mammals, and ship traffic. Each of these sound sources has a unique spectral shape in terms of its SPL-frequency relation (for more details, see Yang et al., 2015; Ma, 2022). These relationships help determine the dominant ambient-noise source for each SPL spectrum, and, in the case of rainfall and surface wind speed, its intensity. Once the SPL spectrum is classified as either dominated by rain or wind, the SPL data at specific frequencies are used to estimate rain rate and wind speed, respectively. For example, if it is classified as rain, the SPL at 5 kHz (SPL_5; in dB) is used to estimate rain rate (RR; mm h^{-1}) using a calibrated SPL_5-RR relationship. PAL-measured acoustic intensity correlates with rain rate, from light to heavy rainfall (Yang et al., 2023). PAL is capable of reliably detecting rain rate of 0.2 mm/hour and has recorded rainfall rates up to 180 mm/hour over the Eastern Tropical Pacific. The sound of drizzle and light rain is actually the most distinctive, so the PAL algorithm performs incredibly well at the lowest rain rates. At wind speeds greater than about 15 m/s, bubbles entrained into the ocean from breaking waves attenuate sound from raindrops hitting the ocean surface, so quantitative rain retrievals become impossible beyond this wind speed.

Since 2010, 58 PALs (3 on moorings and 55 on Argo floats) have been deployed during different field campaigns, in which the reliability of PAL-measured rain rates and wind speeds has been verified against other in-situ measurements from the field campaigns (Ma & Nystuen, 2005; Riser et al., 2019). In general, the uncertainty of PAL-measured rainfall is about 10% (Yang et al., 2015), which is similar to the uncertainty level of other in-situ rainfall measurements given the log-normal behavior of rain rate distributions.

PALs have been mounted on drifting Argo floats and stationary mooring buoys to support recent ocean field campaigns, including NASA's Aquarius Mission (J. Nystuen et al., 2011), Salinity Processes in the Upper Ocean Regional Study campaigns (SPURS-1 and SPURS-2, E. Lindstrom et al., 2015; E. J. Lindstrom et al., 2019), and NOAA's Tropical Pacific Observing System (TPOS, Smith et al., 2019). The PAL collects data along the drifting trajectory of the Argo float. Typically, the Argo float drifts at 1-km depth for approximately 9.5 days between the vertical profiling and surface communication cycles, and the attached PAL records rain rate data at 2-9 minute sampling intervals when rainfall is detected (otherwise, wind speed is recorded). The Argo float typically traverses less than 3 km/day at this depth. PAL has a circular listening area approximately 5 km in diameter when drifting at 1-km depth, making it comparable to spaceborne sensors as they have similar sampling footprint sizes (Yang et al., 2015; Bytheway et al., 2023). PALs on moorings have been deployed at variable depths (e.g., 1 km or a few hundred meters). Their surface sampling diameter is smaller, at scales as about 5 $\times$ the depth.

Figure 1 shows the trajectories or locations of 58 PALs in the current database, spanning the Pacific, North Atlantic, and tropical Indian Oceans. These PALs were deployed at different times (between 2010 and 2020) and their operational period varies (1-4 years), so the number of PALs available at any given time and location is highly variable. The rain rate and wind speed observations from these PALs were recently reprocessed into regular 1-minute intervals and made available for use (Bytheway et al., 2023). The dataset archive can be accessed through NASA EARTHDATA portal (the URL is provided in the Open Research Section), and more details of PALs (e.g., the ID, operational period, drifting extent) can be found in the Supporting Information.

2.2 GPCP Daily Precipitation Products

The GPCP Version 1.3 (hereinafter referred to as "GPCP v1.3") is the first-generation GPCP daily product to provide 1° gridded precipitation estimates over the entire globe from October 1996 to present (Adler et al., 2017). It is based on the One-Degree Daily (1DD) technique, which was detailed in Huffman et al. (2001). This technique consists of two major parts: (1) the Threshold Matched Precipitation Index (TMPI) algorithm, which was used to derive precipitation estimates between 40°N-40°S from low-earth-orbit and geostationary IR datasets, with adjustments made to PMW-derived precipitation occurrence; and (2) the algorithm developed by Susskind et al. (1997), which was used to estimate precipitation over latitudes beyond 40° using the TIROS Operational Vertical Sounder (TOVS; before 2003) or the Advanced Infrared Sounder (AIRS; since 2003) data. Finally, these daily precipitation estimates were calibrated to the GPCP Version 2.3 satellite-gauge monthly product to ensure accuracy and consistency (Adler et al., 2020; Huffman, 1997).

The GPCP Version 3.2 (hereinafter referred to as "GPCP v3.2") aims to improve the accuracy and resolution of precipitation estimates by utilizing the increased number of spaceborne sensors and enhanced merging algorithms in the NASA Global Precipitation Mission (GPM) era. GPCP v3.2 provides daily, global 0.5° gridded precipitation estimates from June 2000 through September 2021 (Huffman et al., 2023a). Compared to GPCP v1.3, the major difference in GPCP v3.2 is the replacement of TMPI algorithm with NASA's Integrated MultisatellitE Retrievals for the GPM mission (IMERG) algorithm (Huffman et al., 2019). IMERG Final Run precipitation estimates are used between 55°N-55°S, while TOVS/AIRS based precipitation estimates are employed at higher latitudes. These precipitation estimates were then calibrated to the new GPCP v3.2 monthly product (Huffman et al., 2023b) that uses the Merged CloudSat, NASA TRMM (Tropical Rainfall Measuring Mission), and NASA GPM climatological precipitation product (MCTG; Behrangi & Song, 2020) over the mid- and high-latitudes oceans and an updated Tropical Composite Climatology (TCC; Adler et al., 2009; Wang et al., 2014) over the tropical oceans for climatological calibration of the GPCP. In addition, GPCP v3.2 contains a diagnostic data field, the probability of liquid phase (PLP; %), which accompanies the precipitation estimates to inform the precipitation phase.

The GPCP v3.2 daily product became available in 2022 with the intention of eventually replacing GPCP v1.3 (Huffman et al., 2023a). While GPCP v1.3 has been widely used and discussed in many climate-, ocean- and water-related studies (e.g., Masunaga et al., 2019; Yu, 2019; Arabzadeh et al., 2020), the validation of GPCP v3.2 is rarely done, especially over oceans due to its recent release and limited reference observations over oceans. The following analyses will be conducted in a comparative manner, with a focus on GPCP v3.2 and its relative performance compared to GPCP v1.3.

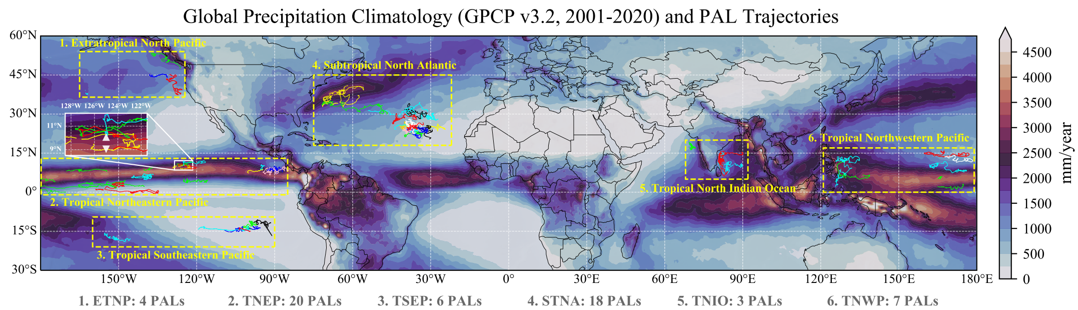

Figure 1. The trajectories of 58 PALs used in this study, on the global precipitation climatology map derived from GPCP v3.2 (2001-2020). Different colors are used for individual PALs to enhance visibility. The two white triangles in the zoomed-in inset show the fixed locations of PALs (on buoy moorings) that were deployed in the tropical Eastern Pacific during SPURS-2.

3 Methodology

The PAL data are matched to the GPCP 1° (v1.3) and 0.5° (v3.2) grids at daily intervals. Each 1-minute PAL rain sample is assigned to a GPCP grid based on its sampling location. All 1-minute PAL data samples within a given GPCP grid are then averaged across the daily time window to compute the daily averaged rain rate from PAL. This matching and averaging procedure is applied to each PAL, resulting in 58 paired PAL-GPCP daily data series. The drifting PALs are unlikely to traverse multiple GPCP grid boxes in a day, as Argo floats typically move less than 3 km/day when drifting at a 1-km depth (Lebedev et al., 2007; Ollitrault & Colin de Verdière, 2014). Our evaluation is limited to liquid precipitation (i.e., rainfall), so the paired PAL-GPCP data with a PLP value (from GPCP v3.2) below 100 are excluded from the subsequent analyses. Approximately 0.8% of the total daily data samples are removed, mainly from the PALs deployed beyond 35°N.

For each PAL, the paired PAL-GPCP daily data are accumulated monthly, and then the daily and monthly data are averaged through the PAL's operational period to calculate the multi-year mean monthly and daily rainfall. We compare these paired daily, monthly, and multi-year mean PAL-GPCP estimates, and evaluate the performance of GPCP in terms of rain detection and rain rate estimation. For rain detection (daily scale only), we calculate the contingency table statistics including the probability of detection (POD), false alarm ratio (FAR), and Heidke skill score (HSS) based on a rain/no-rain detection threshold of 0.5 mm/day. For rain rate estimation, we use relative bias (RB), root-mean-square error (RMSE), normalized root-mean-square error (NRMSE), and the Pearson correlation coefficient (CC). These four metrics are computed either unconditionally (using all PAL-GPCP data including zeros) or conditionally (excluding zeros; i.e., for "hits" only).

We also group the PALs into six regions based on the ocean and latitudes where they are deployed (as shown in Figure 1): (1) 4 PALs in the extratropical North Pacific (ETNP); (2) 20 PALs in the tropical Northeastern Pacific (TNEP); (3) 6 PALs in the tropical Southeastern Pacific (TSEP); (4) 18 PALs in the subtropical North Atlantic (STNA); (5) 3 PALs in the tropical North Indian Ocean (TNIO); and (6) 7 PALs in the tropical Northwestern Pacific (TNWP). The evaluation results will be summarized using this grouping to understand the region-dependent performance of GPCP.

To investigate GPCP's daily performance as a function of rainfall intensity, we calculate the evaluation metrics under various rain detection thresholds (1, 2, 4, ..., 256 mm/day). We combine all the PAL-GPCP daily data for this analysis to ensure sufficient data samples. In addition, two probability distribution functions (PDF), the precipitation occurrence PDF (PDFc) and volume PDF (PDFv) are also computed, following the method detailed in Li et al. (2013).

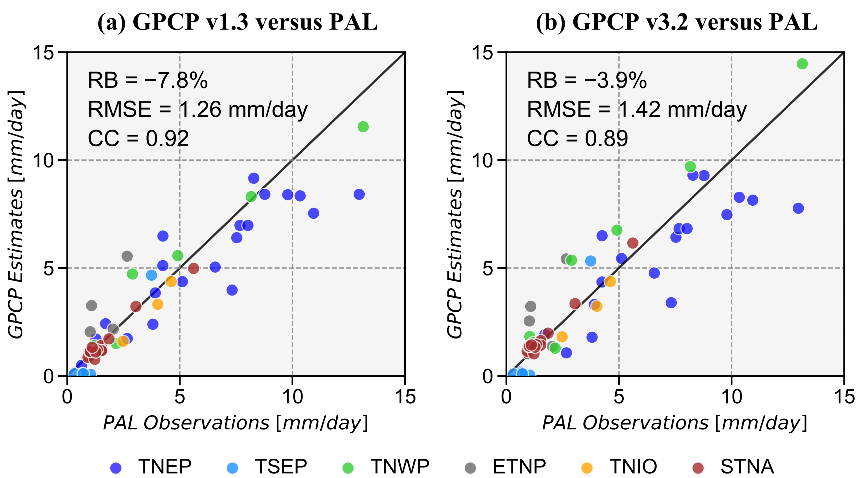

Figure 2. Scatterplots comparing the multi-year mean rain rates (mm/day) estimated by (a) GPCP v1.3 and (b) GPCP v3.2 against PAL observations. Each data point corresponds to one PAL, and the color indicates its group by region.

4 Results

4.1 Comparison of Multi-year Mean

Figure 2 compares the multi-year mean rain rates obtained from the two GPCP products and PALs. The GPCP estimates are highly correlated with in-situ observations, showing the reliability of GPCP products in characterizing rainfall climatology over oceans. The difference between the two GPCP versions is generally small. While GPCP v3.2 has slightly improved the underestimation bias compared to GPCP v1.3, it has introduced additional variability, resulting in larger RMSE and lower CC values. This increased variability can be partially attributed to the higher spatial resolution of GPCP v3.2, which has led to realistic sub-degree variations in precipitation estimates. Despite the overall similarity to v1.3, GPCP v3.2 has region-dependent changes. For example, v3.2 has consistently increased multi-year mean rain rates over the tropical Northwestern Pacific and decreased multi-year mean rain rates at the tropical Northeastern Pacific. Furthermore, the region-dependent visualization in Figure 2 highlights that both GPCP versions have significantly underestimated rainfall over the tropical Southeastern Pacific, which will be further discussed below.

4.2 Seasonality and Monthly Evaluation

GPCP v1.3 and v3.2 perform similarly in representing the seasonality and intra-annual variations of rainfall over most regions (Figs. 3a, c, e-f), and there are no consistent relative improvements in GPCP v3.2 at monthly scale. For example, GPCP v3.2 better captures the seasonality in the second half of the year over the tropical North Indian Ocean (Fig. 3e), but its overestimation bias at the tropical Northwestern Pacific is further increased during the summer (Fig. 3c; also see Table S1 in the Supporting Information).

On the other hand, the GPCP estimates significantly differ from PAL observations in the tropical Southeastern Pacific and extratropical North Pacific, as shown in Figs. 3b and d. Specifically, the two GPCP products consistently underestimate rainfall by about 60% (see Table S1) throughout all months in the tropical Southeastern Pacific. This is likely due to the known limitation of PMW/IR sensors in detecting light and/or shallow convective tropical rainfall, which results in a substantial amount of undetected rain (Behrangi et al., 2012; Schumacher & Houze, 2003). For the high-latitude North Pacific, the discrepancy between GPCP and PAL is most noticeable during winter months (Nov.-Feb.), with GPCP estimates being considerably higher than PAL observations (relative bias exceeds 100%; see Table S1). This is likely because the filtered GPCP daily estimates still contain a considerable amount of solid precipitation due to the imperfect diagnostic variable PLP (Huffman et al., 2023a). The portion of liquid vs. solid is not captured by the PALs since, to date, the PALs and associated algorithms have only been designed for quantifying liquid rainfall (though quantifying snowfall is a future research possibility). Nevertheless, this comparison highlights the challenge of accurately measuring wintertime rainfall with GPCP.

4.3 Daily Rainfall Detection and Estimation Skills

Figure 4 presents the spatial maps of daily evaluation metrics for GPCP products, with detailed statistics provided in Table S2 in the Supporting Information. Compared to the previous version (left panels in Fig. 4), GPCP v3.2 (right panels in Fig. 4) shows remarkable improvement at daily scale. For rainfall detection (Figs. 4a-c and g-i), it consistently reduces FAR and thus increases HSS (also see Table S2). After detection, it further improves rain rate estimation with an increased CC at most locations (Figs. 4f, l). In addition, visual comparison of the bias maps (Figs. 4d, j) suggests that GPCP v3.2 generally overestimates rain rates while GPCP v1.3 is dominated by underestimation.

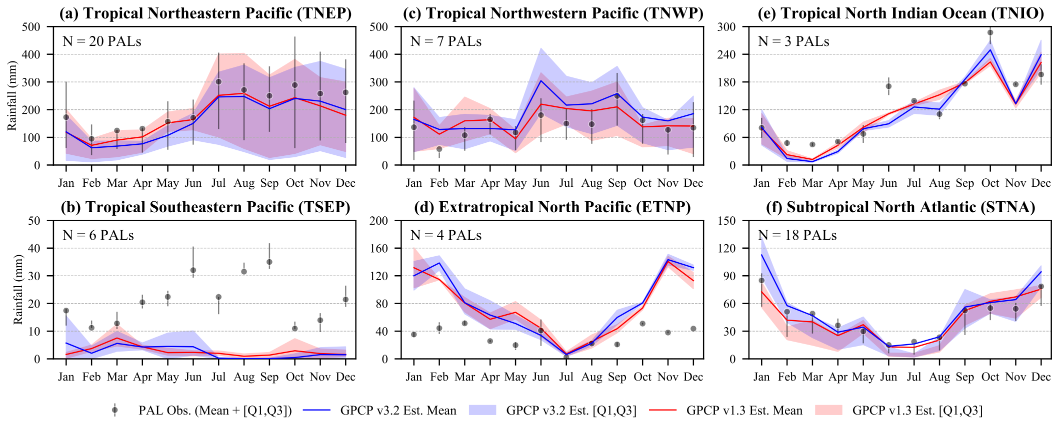

Figure 3. Intra-annual distributions of monthly rainfall estimated from GPCP v1.3, GPCP v3.2 and PAL over different regions (as shown in Fig 1). The comparison includes the mean, and interquartile range (IQR, i.e., the difference between 25% and 75% quantile, [Q1, Q3]) estimates of monthly rainfall, which are calculated from N PALs within each region. Here, N represents the number of PALs.

These relative changes are largely attributed to the incorporation of IMERG Final Run into GPCP v3.2. It suggests that the more direct use of PMW information through IMERG in GPCP V3.2 daily product, results in the observed improvement over GPCP v1.3 that uses TMPI algorithm instead of IMERG.

The rain detection ability of GPCP v3.2 appears to vary across different ocean regions as summarized by HSS (Fig. 4i). The product demonstrates the best detection skills over the tropical North Pacific, where it has the highest probability of detection (POD>0.6) and lowest false alarm rates (FAR<0.4). As it extends towards higher latitudes, either its POD decreases over the North Atlantic (with an IQR of 0.44-0.51; see Table S2) or FAR notably increases over the North Pacific (with an IQR of 0.60-0.62; see Table S2), resulting in degraded detection skills of GPCP v3.2 in these regions. Furthermore, GPCP v3.2 shows its lowest detection potential over the tropical Southeastern Pacific and North Indian Ocean, where it has minimal POD and HSS values.

Once rainfall is detected, GPCP v3.2 estimated daily rain rates correlate well with the PAL data (with a CC greater than 0.5; Fig. 4l) in most areas, except for the tropical Southeastern Pacific. The conditional estimation bias shows a mixed pattern with both negative and positive values in the tropical oceans, while it tends to be dominated by overestimation at higher latitudes, e.g., the North Atlantic and the North Pacific (see Fig. 4j). This overestimation bias peaks in the North Pacific, which is consistent with the monthly results as shown in Fig. 3d.

Similar to Figure 3, Figure 4 also highlights the difference of the rainfall estimates from GPCP and PAL over the tropical Southeastern Pacific and extratropical North Pacific, but with more insights. For tropical Southeastern Pacific, there appears to be more as a "detection" issue since the GPCP and PAL data are barely correlated, exhibiting both low POD and high FAR. In contrast, the extratropical North Pacific is plagued by an overestimation problem, which results in high POD and high FAR. Although the exact reason needs to be further addressed and is outside the scope of this study, this result shows the large uncertainty of precipitation measurements over the two regions.

Figure 5 further shows the improvement of GPCP v3.2 over the prior version as a function of daily rainfall intensity. The PDFs (Figs. 5a-b) indicate that the prior version of GPCP has underestimated the occurrence of both light (<2 mm/day) and heavy rainfall (>20 mm/day), and overestimated the contributions from medium rainfall (4-16 mm/day) in terms of both rain occurrence and volume. In contrast, the PDFs of GPCP v3.2 agree very well with those of PALs, pointing to the success of this new product in accurately representing the full spectrum of rainfall over oceans. GPCP v3.2 shows better rainfall detection skills across all rain intensities (Fig. 5c), especially during heavy rainfall (note the drop of HSS for GPCP v1.3 when rain rate exceeds 8 mm/day). For those detected (i.e., "hits") events, GPCP v3.2 tends to overestimate rainfall under various intensities while GPCP v1.3 tends to largely underestimate it. The correlation decreases with increased rain rates, but the correlation value for GPCP v3.2 is consistently higher (better) than v1.3 by about 0.16.

5 Conclusions

Satellite precipitation products such as GPCP have long served as valuable sources of oceanic precipitation information, which is critical for our understanding of the climate and weather systems, global water and energy cycles, and upper ocean processes. Prior to this study, our knowledge of GPCP precipitation estimation performance over oceans was limited due to insufficient in-situ observations. With recent advances in oceanic observing technology, an increasing number of PALs have been deployed in global oceans to collect minute-scale oceanic rainfall data with a surface sampling area similar to space-borne sensors. These PALs, mostly drifting at 1-km depth along with Argo floats plus a several others on subsurface moorings, cover a broad expanse of ocean areas and many years of time, providing us with an unprecedented opportunity to validate satellite precipitation estimates over oceans. Using 58 PALS as a reference Bytheway et al. (2023) reviewed IMERG, CMORPH, and PDIR-Now, while this study evaluates the GPCP daily products, including the widely-used GPCP v1.3 and the newly released GPCP v3.2. Through a suite of evaluation metrics, we compare the two GPCP products and assess their performance as a function of time scale, region, and rainfall intensity. To the best of our knowledge, this is the first study to validate GPCP daily products using a comprehensive in-situ oceanic dataset of PALs.

GPCP v1.3 and v3.2 perform similarly at multi-year scale. Their multi-year mean rainfall estimates are highly correlated with PAL observations (CC of ∼0.9) with only slight underestimation (7.8 % for v1.3 and 3.9% for v3.2). This demonstrates their reasonable performance in characterizing rainfall climatology over oceans and a slight improvement at multi-year time scales from v3.2. The two versions also capture well the seasonality and intra-annual variations of rainfall over most oceans (e.g., the tropical Northeastern Pacific, tropical Northwestern Pacific, subtropical North Atlantic, and tropical North Indian Ocean) with comparable performance.

When evaluated at daily scale, GPCP v3.2 remarkably outperforms the previous version (v1.3) in terms of rain occurrence and rain intensity. Compared to GPCP v1.3, GPCP v3.2 reduces FAR and thus improves HSS. It also consistently increases CC at most locations. The conditional analysis, which evaluates GPCP's performance as a function of rain intensity, further indicates that GPCP v3.2 consistently exhibits improved skill at different intensities. Its estimated probability distribution functions for rainfall occurrence and volume closely align with those from PALs, whereas GPCP v1.3 underestimates the occurrence of both light (<2 mm/day) and heavy rainfall (>20 mm/day) and overestimates the contributions from medium rainfall (4-16 mm/day).

Our evaluation highlights two regions, the tropical Southeastern Pacific and extratropical North Pacific, where both versions of GPCP products exhibit similar performance and show noticeable differences from PAL observations at multiple time scales. Although the precise causes require detailed analysis outside the scope of this study, the present work highlights the challenges of accurately measuring precipitation with GPCP in these two regions.

This study provides valuable insights into the performance of GPCP daily products over oceans using in-situ observations from 58 PALs across several oceanic regions. It is important to recognize that these PALs are still limited in time and spatial coverage and do not cover the entire global ocean, especially in the southern part. The deployment of additional PALs would certainly increase the opportunity to further evaluate satellite precipitation products, which is needed to understand how best to use them and how to guide their improvements.

Open Research Section

GPCP v1.3 daily data can be obtained from the NOAA National Centers for Environmental Information (NCEI) as part of NOAA Climate Data Record (CDR) Program at `https://www.ncei.noaa.gov/data/global-precipitation-climatology-project-gpcp-daily/access/`. GPCP v3.2 daily data can be accessed from the NASA Goddard Earth Sciences Data and Information Services Center (GES DISC) at `https://disc.gsfc.nasa.gov/datasets/GPCPDAY_3.2/summary`. The PAL dataset archive is currently available at `https://downloads.psl.noaa.gov/psd3/cruises/PAL/`, and will be also available at NASA ERATHDATA portal at `https://doi.org/10.5067/GPMGV/PAL/DATA101`.

Acknowledgments

ZL, EJT and HC were supported in part by the National Aeronautics and Space Administration (NASA) Precipitation Measurement Mission (PMM) through interagency NOAA/NASA agreement 80HQTR20T0049, in part by the NASA Ocean Salinity Science Team (OSST) through interagency NOAA/NASA agreement 80HQTR20T0046, and in part by the National Oceanic and Atmospheric Administration (NOAA) Joint Polar Satellite System (JPSS) Proving Ground and Risk Reduction (PGRR) Program. Funding went to the Cooperative Institute for Research in the Atmosphere (CIRA) at Colorado State University through NOAA grant NA19OAR4320073. AB was supported by NASA MEaSUREs (NNH17ZDA001N-MEASURES) program.

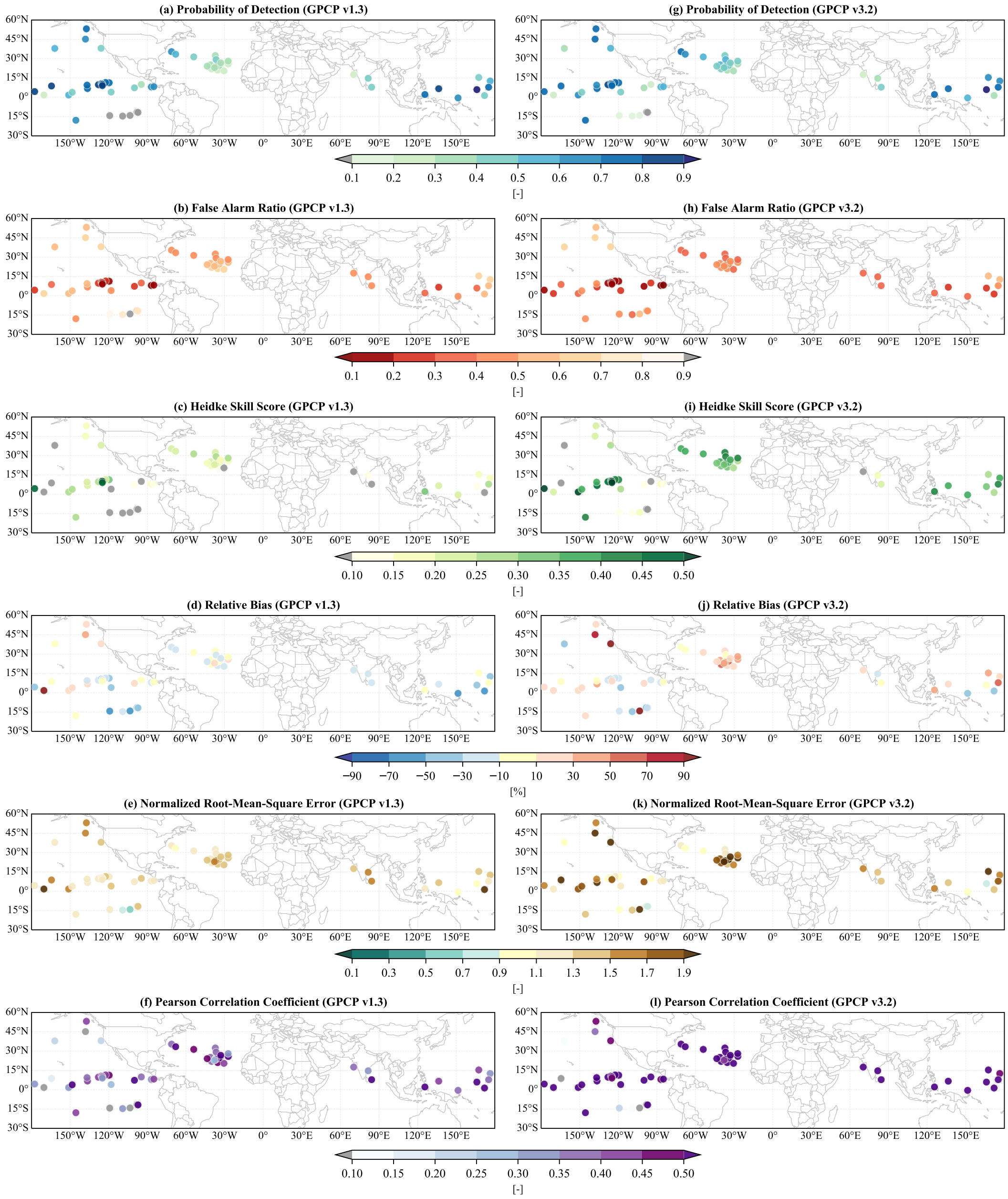

Figure 4. Spatial maps of (a, g) probability of detection (POD), (b, h) false alarm ratio (FAR), (c, i) Heidke skill score (HSS); and conditional (d, j) relative bias (RB), (e, k) normalized root-mean-square error (NRMSE), and (f, l) Pearson's correlation coefficient (CC) for daily GPCP v1.3 (left panels) and GPCP v3.2 (right panels) estimates against PALs. The circles represent the drifting end location of PALs, and rain detection threshold is 0.5 mm/day.

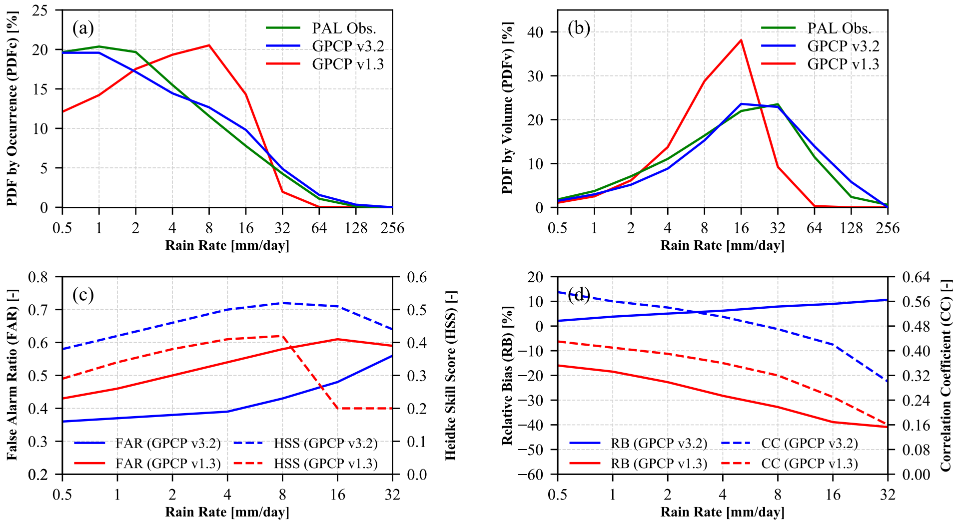

Figure 5. Comparison of (a) probability distribution function by occurrence (PDFc), (b) probability distribution function by volume (PDFv), (c) rainfall detection skills (FAR and HSS), and (d) estimation metrics (RB and CC) as a function of daily rainfall intensity for GPCP products.

References

Adler, R. F., Gu, G., Huffman, G. J., Sapiano, M. R. P., & Wang, J.-J. (2020). GPCP and the Global Characteristics of Precipitation. In V. Levizzani, C. Kidd, D. B. Kirschbaum, C. D. Kummerow, K. Nakamura, & F. J. Turk (Eds.), *Satellite Precipitation Measurement: Volume 2* (pp. 677–697). Springer International Publishing. doi: 10.1007/978-3-030-35798-6_11

Adler, R. F., Huffman, G. J., Chang, A., Ferraro, R., Xie, P.-P., Janowiak, J., ... Nelkin, E. (2003). The Version-2 Global Precipitation Climatology Project (GPCP) Monthly Precipitation Analysis (1979–Present). *Journal of Hydrometeorology*, *4*(6), 1147–1167. doi: 10.1175/1525-7541(2003)004⟨1147:TVGPCP⟩2.0.CO;2

Adler, R. F., Sapiano, M., & Wang, J.-j. (2017, August). *Climate Algorithm Theoretical Basis Document (C-ATBD) for Global Precipitation Climatology Project (GPCP) Daily Analysis Precipitation –GPCP Daily CDR.*

Adler, R. F., Wang, J.-J., Gu, G., & Huffman, G. J. (2009). A Ten-Year Tropical Rainfall Climatology Based on a Composite of TRMM Products. *Journal of the Meteorological Society of Japan. Ser. II*, *87A*, 281–293. doi: 10.2151/jmsj.87A.281

Arabzadeh, A., Ehsani, M. R., Guan, B., Heflin, S., & Behrangi, A. (2020). Global Intercomparison of Atmospheric Rivers Precipitation in Remote Sensing and Reanalysis Products. *Journal of Geophysical Research: Atmospheres*, *125*(21). doi: 10.1029/2020JD033021

Arkin, P. A., & Xie, P. (1994). The Global Precipitation Climatology Project: First Algorithm Intercomparison Project. *Bulletin of the American Meteorological Society*, *75*(3), 401–419. doi: 10.1175/1520-0477(1994)075⟨0401:TGPCPF⟩2.0.CO;2

Behrangi, A., Lebsock, M., Wong, S., & Lambrigtsen, B. (2012). On the Quantification of Oceanic Rainfall Using Spaceborne Sensors. *Journal of Geophysical Research: Atmospheres*, *117*(D20). doi: 10.1029/2012JD017979

Behrangi, A., & Song, Y. (2020). A New Estimate for Oceanic Precipitation Amount and Distribution Using Complementary Precipitation Observations from Space and Comparison with GPCP. *Environmental Research Letters*, *15*(12), 124042. doi: 10.1088/1748-9326/abc6d1

Bolvin, D. T., Huffman, G. J., Nelkin, E. J., & Tan, J. (2021). Comparison of Monthly IMERG Precipitation Estimates with PACRAIN Atoll Observations. *Journal of Hydrometeorology*. doi: 10.1175/JHM-D-20-0202.1

Bowman, K. P. (2005). Comparison of TRMM Precipitation Retrievals with Rain Gauge Data from Ocean Buoys. *Journal of Climate*, *18*(1), 178–190. doi: 10.1175/JCLI3259.1

Bytheway, J. L., Thompson, E. J., Yang, J., & Chen, H. (2023). Evaluating Satellite Precipitation Estimates Over Oceans Using Passive Aquatic Listeners. *Geophysical Research Letters*, *50*(6), e2022GL102087. doi: https://doi.org/10.1029/2022GL102087

Durack, P. (2015). Ocean Salinity and the Global Water Cycle. *Oceanography*, *28*(1), 20–31. doi: 10.5670/oceanog.2015.03

Hartmann, D. L. (2016). Chapter 5 - The Hydrologic Cycle. In D. L. Hartmann (Ed.), *Global Physical Climatology (Second Edition)* (Second Edition ed., p. 131-157). Boston: Elsevier. doi: https://doi.org/10.1016/B978-0-12-328531-7.00005-0

Huffman, G. J. (1997). Estimates of Root-Mean-Square Random Error for Finite Samples of Estimated Precipitation. *Journal of Applied Meteorology*, *36*(9), 1191–1201. doi: 10.1175/1520-0450(1997)036⟨1191:EORMSR⟩2.0.CO;2

Huffman, G. J., Adler, R. F., Arkin, P., Chang, A., Ferraro, R., Gruber, A., ... Schneider, U. (1997). The Global Precipitation Climatology Project (GPCP)

Combined Precipitation Dataset. *Bulletin of the American Meteorological Society*, *78*(1), 5–20. doi: 10.1175/1520-0477(1997)078⟨0005:TGPCPG⟩2.0.CO;2

Huffman, G. J., Adler, R. F., Morrissey, M. M., Bolvin, D. T., Curtis, S., Joyce, R., … Susskind, J. (2001). Global Precipitation at One-Degree Daily Resolution from Multisatellite Observations. *Journal of Hydrometeorology*, *2*(1), 36–50. doi: 10.1175/1525-7541(2001)002⟨0036:GPAODD⟩2.0.CO;2

Huffman, G. J., Alder, R. F., Behrangi, A., Bolvin, D. T., Nelkin, E. J., & Ehsani, M. R. (2023a, January). *Algorithm Theoretical Basis Document (ATBD) for, Global Precipitation Climatology Project Version 3.2 Daily Precipitation Data.*

Huffman, G. J., Alder, R. F., Behrangi, A., Bolvin, D. T., Nelkin, E. J., & Ehsani, M. R. (2023b, January). *Algorithm Theoretical Basis Document (ATBD) for, Global Precipitation Climatology Project Version 3.2 Monthly Precipitation Data.*

Huffman, G. J., Bolvin, D. T., Braithwaite, D., Hsu, K., Joyce, R., Kidd, C., … Xie, P. (2019, March). *Algorithm Theoretical Basis Document (ATBD) Version 06, NASA Global Precipitation Measurement (GPM) Integrated Multi-satellitE Retrievals for GPM (IMERG).*

Kidd, C., Becker, A., Huffman, G. J., Muller, C. L., Joe, P., Skofronick-Jackson, G., & Kirschbaum, D. B. (2017). So, How Much of the Earth's Surface Is Covered by Rain Gauges? *Bulletin of the American Meteorological Society*, *98*(1), 69–78. doi: 10.1175/BAMS-D-14-00283.1

Kidd, C., Huffman, G., Maggioni, V., Chambon, P., & Oki, R. (2021). The Global Satellite Precipitation Constellation: Current Status and Future Requirements. *Bulletin of the American Meteorological Society*, *102*(10), E1844–E1861. doi: 10.1175/BAMS-D-20-0299.1

Klepp, C., Michel, S., Protat, A., Burdanowitz, J., Albern, N., Kähnert, M., … Buehler, S. A. (2018). Oceanrain, A New In-situ Shipboard Global Ocean Surface-reference Dataset of All Water Cycle Components. *Scientific Data*, *5*(1), 1–22.

Lagerloef, G., Schmitt, R., Schanze, J., & Kao, H.-Y. (2010). The Ocean and the Global Water Cycle. *Oceanography*, *23*(4), 82–93. doi: 10.5670/oceanog.2010.07

Lebedev, K., Yoshinari, H., Maximenko, N., & Hacker, P. (2007). *YoMaHa'07: Velocity Data Assessed from Trajectories of Argo Floats at Parking Level and at the Sea Surface* (Tech. Rep. No. 4(2)). IPRC Technical Note.

Levizzani, V., Kidd, C., Aonashi, K., Bennartz, R., Ferraro, R. R., Huffman, G. J., … Wang, N. (2018). The Activities of the International Precipitation Working Group. *Quarterly Journal of the Royal Meteorological Society*, *144*(S1), 3–15. doi: 10.1002/qj.3214

Li, Z., Yang, D., & Hong, Y. (2013). Multi-scale Evaluation of High-resolution Multi-sensor Blended Global Precipitation Products over the Yangtze River. *Journal of Hydrology*, *500*, 157–169. doi: 10.1016/j.jhydrol.2013.07.023

Lindstrom, E., Bryan, F., & Schmitt, R. (2015). SPURS: Salinity Processes in the Upper-ocean Regional Study. *Oceanography*, *28*(1), 14–19.

Lindstrom, E. J., Edson, J. B., Schanze, J. J., & Shcherbina, A. Y. (2019). SPURS-2: Salinity Processes in the Upper-Ocean Regional Study 2 – The Eastern Equatorial Pacific Experiment. *Oceanography*, 6. doi: https://doi.org/10.5670/oceanog.2019.207

Ma, B. B. (2022). Rainfall at Sea: Using the Underwater Sounds of Raindrops as a Rain Gauge for Weather and Climate. *Acoustics Today*, *18*(2), 62. doi: 10.1121/AT.2022.18.2.62

Ma, B. B., & Nystuen, J. A. (2005). Passive Acoustic Detection and Measurement of Rainfall at Sea. *Journal of Atmospheric and Oceanic Technology*, *22*.

Masunaga, H., Schröder, M., Furuzawa, F. A., Kummerow, C., Rustemeier, E., & Schneider, U. (2019). Inter-product Biases in Global Precipita-

tion Extremes. *Environmental Research Letters*, *14*(12), 125016. doi: 10.1088/1748-9326/ab5da9
Moum, J., & Smyth, W. (2019). Upper Ocean Mixing. In *Encyclopedia of Ocean Sciences* (pp. 71–79). Elsevier. doi: 10.1016/B978-0-12-409548-9.11573-8
Nystuen, J., Riser, S., Wen, T., & Swift, D. (2011). Interpreted Acoustic Ocean Observations from Argo Floats. *The Journal of the Acoustical Society of America*, *129*(4), 2400–2400. doi: 10.1121/1.3587814
Nystuen, J. A., Anagnostou, M. N., Anagnostou, E. N., & Papadopoulos, A. (2015). Monitoring Greek Seas Using Passive Underwater Acoustics. *Journal of Atmospheric and Oceanic Technology*, *32*(2), 334–349. doi: 10.1175/JTECH-D-13-00264.1
O'Kane, T. J., Monselesan, D. P., & Maes, C. (2016). On the Stability and Spatiotemporal Variance Distribution of Salinity in the Upper Ocean. *Journal of Geophysical Research: Oceans*, *121*(6), 4128–4148. doi: 10.1002/2015JC011523
Ollitrault, M., & Colin de Verdière, A. (2014). The Ocean General Circulation near 1000-m Depth. *Journal of Physical Oceanography*, *44*(1), 384–409. doi: 10.1175/JPO-D-13-030.1
Pfeifroth, U., Mueller, R., & Ahrens, B. (2013). Evaluation of Satellite-Based and Reanalysis Precipitation Data in the Tropical Pacific. *Journal of Applied Meteorology and Climatology*, *52*(3), 634–644. doi: 10.1175/JAMC-D-12-049.1
Riser, S., Yang, J., & Drucker, R. (2019). Observations of Large-Scale Rainfall, Wind, and Sea Surface Salinity Variability in the Eastern Tropical Pacific. *Oceanography*, *32*(2), 42–49. doi: 10.5670/oceanog.2019.211
Roemmich, D., Alford, M. H., Claustre, H., Johnson, K., King, B., Moum, J., … Yasuda, I. (2019). On the Future of Argo: A Global, Full-Depth, Multi-Disciplinary Array. *Frontiers in Marine Science*, *6*, 439. doi: 10.3389/fmars.2019.00439
Rutledge, S., Chandrasekar, V., Fuchs, B., George, J., Junyent, F., Kennedy, P., & Dolan, B. (2019). Deployment of the SEA-POL C-band Polarimetric Radar to SPURS-2. *Oceanography*, *32*(2), 50–57. doi: 10.5670/oceanog.2019.212
Sallée, J.-B., Pellichero, V., Akhoudas, C., Pauthenet, E., Vignes, L., Schmidtko, S., … Kuusela, M. (2021). Summertime increases in upper-ocean stratification and mixed-layer depth. *Nature*, *591*(7851), 592–598. doi: 10.1038/s41586-021-03303-x
Sapiano, M. R. P., & Arkin, P. A. (2009). An Intercomparison and Validation of High-Resolution Satellite Precipitation Estimates with 3-Hourly Gauge Data. *Journal of Hydrometeorology*, *10*(1), 149–166. doi: 10.1175/2008JHM1052.1
Schmitt, R. W. (1995). The Ocean Component of the Global Water Cycle. *Reviews of Geophysics*, *33*(S2), 1395–1409. doi: 10.1029/95RG00184
Schumacher, C., & Houze, R. A. (2003). The TRMM Precipitation Radar's View of Shallow, Isolated Rain. *Journal of Applied Meteorology*, *42*(10), 1519–1524. doi: 10.1175/1520-0450(2003)042⟨1519:TTPRVO⟩2.0.CO;2
Smith, N., Kessler, W. S., Cravatte, S., Sprintall, J., Wijffels, S., Cronin, M. F., … Brunner, S. (2019). Tropical Pacific Observing System. *Frontiers in Marine Science*, *6*, 31. doi: 10.3389/fmars.2019.00031
Susskind, J., Piraino, P., Rokke, L., Iredell, L., & Mehta, A. (1997). Characteristics of the TOVS Pathfinder Path A Dataset. *Bulletin of the American Meteorological Society*, *78*(7), 1449–1472. doi: 10.1175/1520-0477(1997)078⟨1449:COTTPP⟩2.0.CO;2
Trenberth, K. E., Smith, L., Qian, T., Dai, A., & Fasullo, J. (2007). Estimates of the Global Water Budget and Its Annual Cycle Using Observational and Model Data. *Journal of Hydrometeorology*, *8*(4), 758–769. doi: 10.1175/JHM600.1
Wang, J.-J., Adler, R. F., Huffman, G. J., & Bolvin, D. (2014). An Updated TRMM

Composite Climatology of Tropical Rainfall and Its Validation. *Journal of Climate*, *27*(1), 273–284. doi: 10.1175/JCLI-D-13-00331.1

Yang, J., Nystuen, J. A., Riser, S. C., & Thorsos, E. I. (2023). Open Ocean Ambient Noise Data in the Frequency Band of 100 Hz–50 kHz from the Pacific Ocean. *JASA Express Letters*, *3*(3), 036001. doi: 10.1121/10.0017349

Yang, J., Riser, S., Nystuen, J., Asher, W., & Jessup, A. (2015). Regional Rainfall Measurements Using the Passive Aquatic Listener During the SPURS Field Campaign. *Oceanography*, *28*(1), 124–133. doi: 10.5670/oceanog.2015.10

Yu, L. (2011). A Global Relationship Between the Ocean Water Cycle and Near-surface Salinity. *Journal of Geophysical Research: Oceans*, *116*(C10). doi: https://doi.org/10.1029/2010JC006937

Yu, L. (2019). Global Air–Sea Fluxes of Heat, Fresh Water, and Momentum: Energy Budget Closure and Unanswered Questions. *Annual Review of Marine Science*, *11*(1), 227-248. doi: 10.1146/annurev-marine-010816-060704

Performance of GPCP Products Over Oceans: Evaluation Using Passive Aquatic Listeners

Zhe Li[1], Elizabeth J. Thompson[2], Ali Behrangi[3], Haonan Chen[1], Jie Yang[4]

[1]Department of Electrical and Computer Engineering, Colorado State University, Fort Collins, CO 80523, USA
[2]NOAA Physical Sciences Laboratory, Boulder, CO 80305, USA
[3]Department of Hydrology and Atmospheric Sciences, The University of Arizona, Tucson, AZ 85721, USA
[4]Applied Physics Laboratory, University of Washington, Seattle, WA 98105, USA

Key Points:

- Passive Aquatic Listeners (PALs) are used to validate GPCP products over global oceans.
- Newly released GPCP Version 3.2 and the previous Version 1.3 daily products are compared.
- The performance of GPCP products depends on time scale, location, and rainfall intensity.

Corresponding author: Dr. Zhe Li, `zhe.li@colostate.edu`

Abstract

Passive Aquatic Listeners (PALs) have been increasingly deployed to collect minute-scale surface oceanic rainfall and wind information, with a sampling area similar to the spaceborne sensor footprints. This provides an unprecedented opportunity to validate satellite precipitation products over oceans. This study evaluates the Global Precipitation Climatology Project (GPCP) daily products, including the widely-used GPCP v1.3 and the newly released GPCP v3.2, over oceans using 58 PALs as references. The study shows that the GPCP performance depends on time scale, region, and rainfall intensity. The two versions of GPCP perform similarly at multi-year and monthly scales, while GPCP v3.2 shows substantial improvements in representing rain occurrence and rain intensity at daily scale. The results also highlight the challenge of precipitation measurement over certain regions such as the tropical Northeastern Pacific and extratropical North Pacific, where both versions of the GPCP products perform similarly but exhibit noticeable differences compared to PAL observations.

Plain Language Summary

Satellites are the main instruments to quantify precipitation over the ocean, but it is difficult to check their accuracy because we do not have many rain gauges over oceans to compare with satellites. The Passive Aquatic Listener (PAL) is “the underwater phone” to listen to the sound generated when raindrops hit the sea surface. The PAL estimates rain rates based on the loudness of the sound at each frequency. This is similar to listening to the rain under a tin roof. PAL can drift with ocean currents for years, so it can collect rainfall data over a large ocean area. The Global Precipitation Climatology Project (GPCP) product is a popular long-term satellite-based precipitation data record to study climate, water cycle, and the ocean. This study uses PAL observations to evaluate the performance of GPCP’s latest two versions: v1.3, and the newly released GPCP v3.2. The results show that the new product is better than the old product in estimating daily rainfall, while they are similar when estimating monthly and multi-year rainfall. We also notice that they provide similar estimates, which are both quite different from PAL observations, over the tropical Northeastern Pacific and extratropical North Pacific.

1 Introduction

Precipitation is an essential component of the global water and energy cycles. For this reason, it has long been recognized that accurate knowledge of the time, amount, and distribution of precipitation plays a fundamental role in understanding the Earth’s climate system (Hartmann, 2016). As the largest reservoir of water in this system, the oceans receive over 75% of global precipitation and contribute approximately 85% of atmospheric water vapor through evaporation (Lagerloef et al., 2010). The difference between precipitation and evaporation (also known as the ocean-atmosphere freshwater flux) directly affects the upper ocean temperature, salinity, density, stability, and turbulence (Moum & Smyth, 2019; Sallée et al., 2021; O’Kane et al., 2016), This influences oceanic and atmospheric circulations and heat content, which regulate climate variability across multiple scales (Schmitt, 1995; Durack, 2015). Despite its importance, oceanic precipitation remains one of the least understood elements in the Earth’s climate system due to the lack of in-situ observations over oceans (Trenberth et al., 2007; Kidd et al., 2017).

To fill this gap, satellites have played a major role to quantify oceanic precipitation. The precipitation-capable spaceborne sensors include infrared (IR), passive microwave (PMW) imagers/sounders, and radars. Since each type of sensor has its own strengths and limitations, today’s satellite-based precipitation products are built upon a multi-sensor approach, which integrates the measurements from a constellation of spaceborne sensors to maximize the accuracy, coverage, and resolution of precipitation estimates on a global scale (Kidd et al., 2021). Furthermore, long-term climate records of global precipitation can only be achieved through such a multi-sensor strategy (Levizzani et al., 2018). In this regard, the Global Precipitation Climatology Project (GPCP) was developed by merging PMW/IR sensors and rain gauges (over land) to provide this information to the international community. For a long time, GPCP linked to the World Climate Research Programme (WCRP) and Global Energy and Water Experiment (GEWEX) activities (Adler et al., 2020).

GPCP was first introduced in the mid-1990s (Arkin & Xie, 1994; Huffman et al., 1997), and since then, it has undergone several iterations to improve the input data sources, merging algorithms, and resolution (Huffman et al., 2001; Adler et al., 2003; Huffman et al., 2023a). GPCP products have been widely used to study the precipitation climatology and the hydrologic cycle (e.g., Yu, 2011; Lagerloef et al., 2010). However, validating satellite-based precipitation estimates, including GPCP, over oceans remains challenging. The in-situ reference data for validation are generally limited to rain gauges, which are only available from a small number of atoll/islands sites, moored buoys, and research vessels (Bowman, 2005; Sapiano & Arkin, 2009; Pfeifroth et al., 2013; Bolvin et al., 2021). Additionally, rain gauges may provide an incomplete representation of precipitation compared to satellite data, due to the point sampling nature of gauges relative to satellite grid box estimates that are several kilometers wide (Kidd et al., 2021). To overcome data limitations at sea, several other ocean-specific precipitation instruments have emerged, such as ship-based optical disdrometers (Klepp et al., 2018), ship-based motion-stabilized radars (Rutledge et al., 2019), and the subsurface Passive Aquatic Listeners (PAL; Ma & Nystuen, 2005; Yang et al., 2015).

Different from rain gauge or ship-based sensors, PAL is an underwater acoustic sensor (hydrophone) typically mounted on drifting Argo floats (Roemmich et al., 2019), which can collect oceanic rainfall and wind information at minute-scale over a large domain. In addition, a PAL has a sampling area similar to the footprint of spaceborne sensors, making it more comparable to satellite data. Since 2010, 58 PALs have been deployed over different oceans, and their observations were recently reprocessed and made available for use (Yang et al., 2015; Bytheway et al., 2023). In this study, we leverage this newly-available oceanic rainfall dataset to validate GPCP daily products over the ocean. To our best knowledge, this work represents the most expansive validation of GPCP daily data over oceans because it uses the distributed set of in-situ observations available from the state-of-the-art multiyear PAL database.

2 Data

2.1 Passive Aquatic Listeners

PAL is an innovative acoustic sensor, a hydrophone, designed to measure rain rate and wind speed routinely over the ocean (J. A. Nystuen et al., 2015; Yang et al., 2015). It collects underwater ambient-noise time series at different frequencies and converts them into a multi-frequency (1-50 kHz) spectrum of sound pressure levels (SPL). The overall SPL can be attributed to different sources of ocean ambient sound such as raindrops, surface wind, wave breaking, marine mammals, and ship traffic. Each of these sound sources has a unique spectral shape in terms of its SPL-frequency relation (for more details, see Yang et al., 2015; Ma, 2022). These relationships help determine the dominant ambient-noise source for each SPL spectrum, and, in the case of rainfall and surface wind speed, its intensity. Once the SPL spectrum is classified as either dominated by rain or wind, the SPL data at specific frequencies are used to estimate rain rate and wind speed, respectively. For example, if it is classified as rain, the SPL at 5 kHz (SPL_5; in dB) is used to estimate rain rate (RR; mm h^{-1}) using a calibrated SPL_5-RR relationship. PAL-measured acoustic intensity correlates with rain rate, from light to heavy rainfall (Yang et al., 2023). PAL is capable of reliably detecting rain rate of 0.2 mm/hour and has recorded rainfall rates up to 180 mm/hour over the Eastern Tropical Pacific. The sound of drizzle and light rain is actually the most distinctive, so the PAL algorithm performs incredibly well at the lowest rain rates. At wind speeds greater than about 15 m/s, bubbles entrained into the ocean from breaking waves attenuate sound from raindrops hitting the ocean surface, so quantitative rain retrievals become impossible beyond this wind speed.

Since 2010, 58 PALs (3 on moorings and 55 on Argo floats) have been deployed during different field campaigns, in which the reliability of PAL-measured rain rates and wind speeds has been verified against other in-situ measurements from the field campaigns (Ma & Nystuen, 2005; Riser et al., 2019). In general, the uncertainty of PAL-measured rainfall is about 10% (Yang et al., 2015), which is similar to the uncertainty level of other in-situ rainfall measurements given the log-normal behavior of rain rate distributions.

PALs have been mounted on drifting Argo floats and stationary mooring buoys to support recent ocean field campaigns, including NASA's Aquarius Mission (J. Nystuen et al., 2011), Salinity Processes in the Upper Ocean Regional Study campaigns (SPURS-1 and SPURS-2, E. Lindstrom et al., 2015; E. J. Lindstrom et al., 2019), and NOAA's Tropical Pacific Observing System (TPOS, Smith et al., 2019). The PAL collects data along the drifting trajectory of the Argo float. Typically, the Argo float drifts at 1-km depth for approximately 9.5 days between the vertical profiling and surface communication cycles, and the attached PAL records rain rate data at 2-9 minute sampling intervals when rainfall is detected (otherwise, wind speed is recorded). The Argo float typically traverses less than 3 km/day at this depth. PAL has a circular listening area approximately 5 km in diameter when drifting at 1-km depth, making it comparable to spaceborne sensors as they have similar sampling footprint sizes (Yang et al., 2015; Bytheway et al., 2023). PALs on moorings have been deployed at variable depths (e.g., 1 km or a few hundred meters). Their surface sampling diameter is smaller, at scales as about 5 $\times$ the depth.

Figure 1 shows the trajectories or locations of 58 PALs in the current database, spanning the Pacific, North Atlantic, and tropical Indian Oceans. These PALs were deployed at different times (between 2010 and 2020) and their operational period varies (1-4 years), so the number of PALs available at any given time and location is highly variable. The rain rate and wind speed observations from these PALs were recently reprocessed into regular 1-minute intervals and made available for use (Bytheway et al., 2023). The dataset archive can be accessed through NASA EARTHDATA portal (the URL is provided in the Open Research Section), and more details of PALs (e.g., the ID, operational period, drifting extent) can be found in the Supporting Information.

2.2 GPCP Daily Precipitation Products

The GPCP Version 1.3 (hereinafter referred to as "GPCP v1.3") is the first-generation GPCP daily product to provide 1° gridded precipitation estimates over the entire globe from October 1996 to present (Adler et al., 2017). It is based on the One-Degree Daily (1DD) technique, which was detailed in Huffman et al. (2001). This technique consists of two major parts: (1) the Threshold Matched Precipitation Index (TMPI) algorithm, which was used to derive precipitation estimates between 40°N-40°S from low-earth-orbit and geostationary IR datasets, with adjustments made to PMW-derived precipitation occurrence; and (2) the algorithm developed by Susskind et al. (1997), which was used to estimate precipitation over latitudes beyond 40° using the TIROS Operational Vertical Sounder (TOVS; before 2003) or the Advanced Infrared Sounder (AIRS; since 2003) data. Finally, these daily precipitation estimates were calibrated to the GPCP Version 2.3 satellite-gauge monthly product to ensure accuracy and consistency (Adler et al., 2020; Huffman, 1997).

The GPCP Version 3.2 (hereinafter referred to as "GPCP v3.2") aims to improve the accuracy and resolution of precipitation estimates by utilizing the increased number of spaceborne sensors and enhanced merging algorithms in the NASA Global Precipitation Mission (GPM) era. GPCP v3.2 provides daily, global 0.5° gridded precipitation estimates from June 2000 through September 2021 (Huffman et al., 2023a). Compared to GPCP v1.3, the major difference in GPCP v3.2 is the replacement of TMPI algorithm with NASA's Integrated MultisatellitE Retrievals for the GPM mission (IMERG) algorithm (Huffman et al., 2019). IMERG Final Run precipitation estimates are used between 55°N-55°S, while TOVS/AIRS based precipitation estimates are employed at higher latitudes. These precipitation estimates were then calibrated to the new GPCP v3.2 monthly product (Huffman et al., 2023b) that uses the Merged CloudSat, NASA TRMM (Tropical Rainfall Measuring Mission), and NASA GPM climatological precipitation product (MCTG; Behrangi & Song, 2020) over the mid- and high-latitudes oceans and an updated Tropical Composite Climatology (TCC; Adler et al., 2009; Wang et al., 2014) over the tropical oceans for climatological calibration of the GPCP. In addition, GPCP v3.2 contains a diagnostic data field, the probability of liquid phase (PLP; %), which accompanies the precipitation estimates to inform the precipitation phase.

The GPCP v3.2 daily product became available in 2022 with the intention of eventually replacing GPCP v1.3 (Huffman et al., 2023a). While GPCP v1.3 has been widely used and discussed in many climate-, ocean- and water-related studies (e.g., Masunaga et al., 2019; Yu, 2019; Arabzadeh et al., 2020), the validation of GPCP v3.2 is rarely done, especially over oceans due to its recent release and limited reference observations over oceans. The following analyses will be conducted in a comparative manner, with a focus on GPCP v3.2 and its relative performance compared to GPCP v1.3.

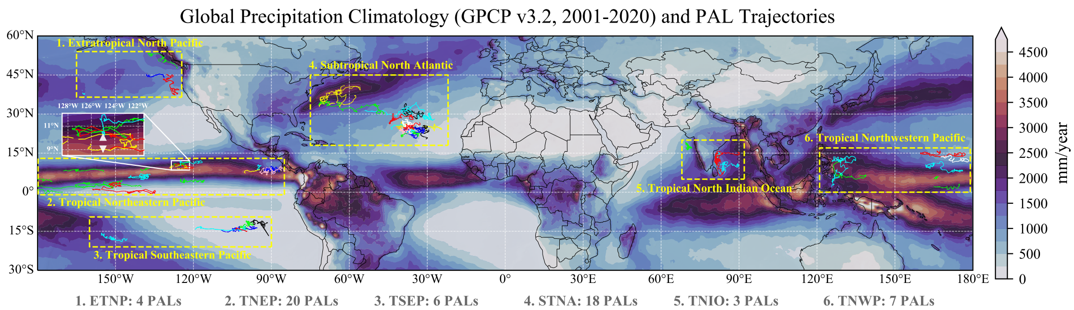

Figure 1. The trajectories of 58 PALs used in this study, on the global precipitation climatology map derived from GPCP v3.2 (2001-2020). Different colors are used for individual PALs to enhance visibility. The two white triangles in the zoomed-in inset show the fixed locations of PALs (on buoy moorings) that were deployed in the tropical Eastern Pacific during SPURS-2.

3 Methodology

The PAL data are matched to the GPCP 1° (v1.3) and 0.5° (v3.2) grids at daily intervals. Each 1-minute PAL rain sample is assigned to a GPCP grid based on its sampling location. All 1-minute PAL data samples within a given GPCP grid are then averaged across the daily time window to compute the daily averaged rain rate from PAL. This matching and averaging procedure is applied to each PAL, resulting in 58 paired PAL-GPCP daily data series. The drifting PALs are unlikely to traverse multiple GPCP grid boxes in a day, as Argo floats typically move less than 3 km/day when drifting at a 1-km depth (Lebedev et al., 2007; Ollitrault & Colin de Verdière, 2014). Our evaluation is limited to liquid precipitation (i.e., rainfall), so the paired PAL-GPCP data with a PLP value (from GPCP v3.2) below 100 are excluded from the subsequent analyses. Approximately 0.8% of the total daily data samples are removed, mainly from the PALs deployed beyond 35°N.

For each PAL, the paired PAL-GPCP daily data are accumulated monthly, and then the daily and monthly data are averaged through the PAL's operational period to calculate the multi-year mean monthly and daily rainfall. We compare these paired daily, monthly, and multi-year mean PAL-GPCP estimates, and evaluate the performance of GPCP in terms of rain detection and rain rate estimation. For rain detection (daily scale only), we calculate the contingency table statistics including the probability of detection (POD), false alarm ratio (FAR), and Heidke skill score (HSS) based on a rain/no-rain detection threshold of 0.5 mm/day. For rain rate estimation, we use relative bias (RB), root-mean-square error (RMSE), normalized root-mean-square error (NRMSE), and the Pearson correlation coefficient (CC). These four metrics are computed either unconditionally (using all PAL-GPCP data including zeros) or conditionally (excluding zeros; i.e., for "hits" only).

We also group the PALs into six regions based on the ocean and latitudes where they are deployed (as shown in Figure 1): (1) 4 PALs in the extratropical North Pacific (ETNP); (2) 20 PALs in the tropical Northeastern Pacific (TNEP); (3) 6 PALs in the tropical Southeastern Pacific (TSEP); (4) 18 PALs in the subtropical North Atlantic (STNA); (5) 3 PALs in the tropical North Indian Ocean (TNIO); and (6) 7 PALs in the tropical Northwestern Pacific (TNWP). The evaluation results will be summarized using this grouping to understand the region-dependent performance of GPCP.

To investigate GPCP's daily performance as a function of rainfall intensity, we calculate the evaluation metrics under various rain detection thresholds (1, 2, 4, ..., 256 mm/day). We combine all the PAL-GPCP daily data for this analysis to ensure sufficient data samples. In addition, two probability distribution functions (PDF), the precipitation occurrence PDF (PDFc) and volume PDF (PDFv) are also computed, following the method detailed in Li et al. (2013).

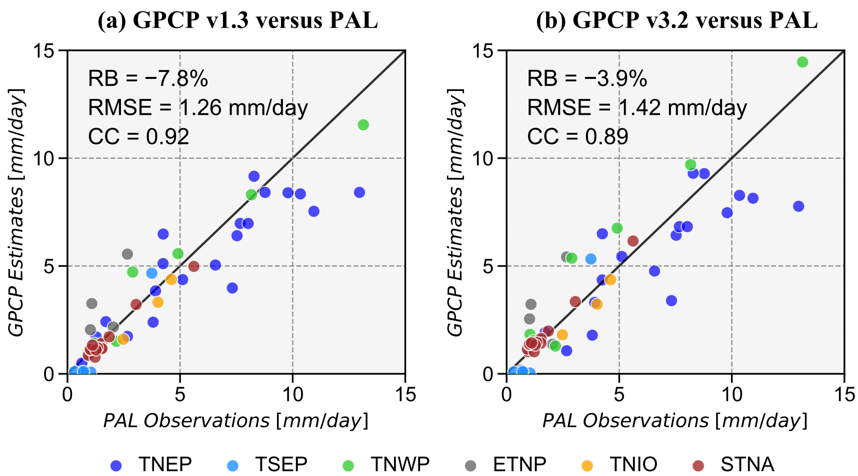

Figure 2. Scatterplots comparing the multi-year mean rain rates (mm/day) estimated by (a) GPCP v1.3 and (b) GPCP v3.2 against PAL observations. Each data point corresponds to one PAL, and the color indicates its group by region.

4 Results

4.1 Comparison of Multi-year Mean

Figure 2 compares the multi-year mean rain rates obtained from the two GPCP products and PALs. The GPCP estimates are highly correlated with in-situ observations, showing the reliability of GPCP products in characterizing rainfall climatology over oceans. The difference between the two GPCP versions is generally small. While GPCP v3.2 has slightly improved the underestimation bias compared to GPCP v1.3, it has introduced additional variability, resulting in larger RMSE and lower CC values. This increased variability can be partially attributed to the higher spatial resolution of GPCP v3.2, which has led to realistic sub-degree variations in precipitation estimates. Despite the overall similarity to v1.3, GPCP v3.2 has region-dependent changes. For example, v3.2 has consistently increased multi-year mean rain rates over the tropical Northwestern Pacific and decreased multi-year mean rain rates at the tropical Northeastern Pacific. Furthermore, the region-dependent visualization in Figure 2 highlights that both GPCP versions have significantly underestimated rainfall over the tropical Southeastern Pacific, which will be further discussed below.

4.2 Seasonality and Monthly Evaluation

GPCP v1.3 and v3.2 perform similarly in representing the seasonality and intra-annual variations of rainfall over most regions (Figs. 3a, c, e-f), and there are no consistent relative improvements in GPCP v3.2 at monthly scale. For example, GPCP v3.2 better captures the seasonality in the second half of the year over the tropical North Indian Ocean (Fig. 3e), but its overestimation bias at the tropical Northwestern Pacific is further increased during the summer (Fig. 3c; also see Table S1 in the Supporting Information).

On the other hand, the GPCP estimates significantly differ from PAL observations in the tropical Southeastern Pacific and extratropical North Pacific, as shown in Figs. 3b and d. Specifically, the two GPCP products consistently underestimate rainfall by about 60% (see Table S1) throughout all months in the tropical Southeastern Pacific. This is likely due to the known limitation of PMW/IR sensors in detecting light and/or shallow convective tropical rainfall, which results in a substantial amount of undetected rain (Behrangi et al., 2012; Schumacher & Houze, 2003). For the high-latitude North Pacific, the discrepancy between GPCP and PAL is most noticeable during winter months (Nov.-Feb.), with GPCP estimates being considerably higher than PAL observations (relative bias exceeds 100%; see Table S1). This is likely because the filtered GPCP daily estimates still contain a considerable amount of solid precipitation due to the imperfect diagnostic variable PLP (Huffman et al., 2023a). The portion of liquid vs. solid is not captured by the PALs since, to date, the PALs and associated algorithms have only been designed for quantifying liquid rainfall (though quantifying snowfall is a future research possibility). Nevertheless, this comparison highlights the challenge of accurately measuring wintertime rainfall with GPCP.

4.3 Daily Rainfall Detection and Estimation Skills

Figure 4 presents the spatial maps of daily evaluation metrics for GPCP products, with detailed statistics provided in Table S2 in the Supporting Information. Compared to the previous version (left panels in Fig. 4), GPCP v3.2 (right panels in Fig. 4) shows remarkable improvement at daily scale. For rainfall detection (Figs. 4a-c and g-i), it consistently reduces FAR and thus increases HSS (also see Table S2). After detection, it further improves rain rate estimation with an increased CC at most locations (Figs. 4f, l). In addition, visual comparison of the bias maps (Figs. 4d, j) suggests that GPCP v3.2 generally overestimates rain rates while GPCP v1.3 is dominated by underestimation.

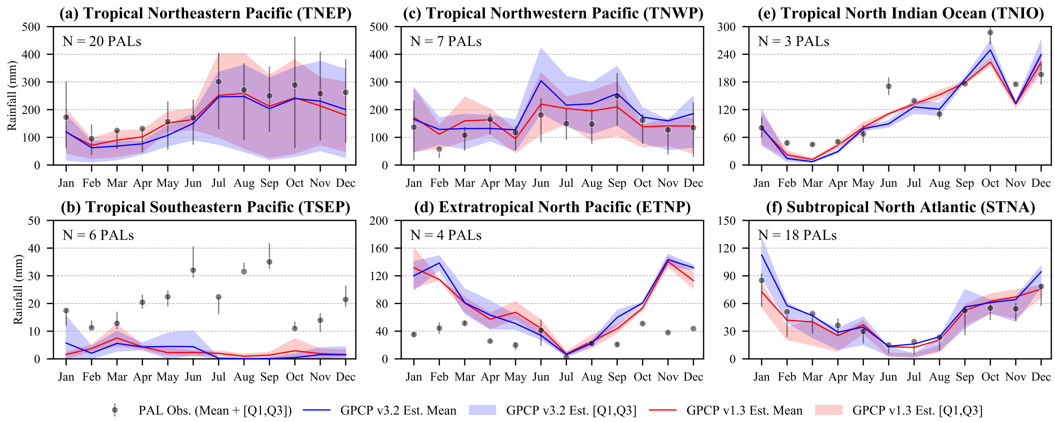

Figure 3. Intra-annual distributions of monthly rainfall estimated from GPCP v1.3, GPCP v3.2 and PAL over different regions (as shown in Fig 1). The comparison includes the mean, and interquartile range (IQR, i.e., the difference between 25% and 75% quantile, [Q1, Q3]) estimates of monthly rainfall, which are calculated from N PALs within each region. Here, N represents the number of PALs.

These relative changes are largely attributed to the incorporation of IMERG Final Run into GPCP v3.2. It suggests that the more direct use of PMW information through IMERG in GPCP V3.2 daily product, results in the observed improvement over GPCP v1.3 that uses TMPI algorithm instead of IMERG.

The rain detection ability of GPCP v3.2 appears to vary across different ocean regions as summarized by HSS (Fig. 4i). The product demonstrates the best detection skills over the tropical North Pacific, where it has the highest probability of detection (POD>0.6) and lowest false alarm rates (FAR<0.4). As it extends towards higher latitudes, either its POD decreases over the North Atlantic (with an IQR of 0.44-0.51; see Table S2) or FAR notably increases over the North Pacific (with an IQR of 0.60-0.62; see Table S2), resulting in degraded detection skills of GPCP v3.2 in these regions. Furthermore, GPCP v3.2 shows its lowest detection potential over the tropical Southeastern Pacific and North Indian Ocean, where it has minimal POD and HSS values.

Once rainfall is detected, GPCP v3.2 estimated daily rain rates correlate well with the PAL data (with a CC greater than 0.5; Fig. 4l) in most areas, except for the tropical Southeastern Pacific. The conditional estimation bias shows a mixed pattern with both negative and positive values in the tropical oceans, while it tends to be dominated by overestimation at higher latitudes, e.g., the North Atlantic and the North Pacific (see Fig. 4j). This overestimation bias peaks in the North Pacific, which is consistent with the monthly results as shown in Fig. 3d.

Similar to Figure 3, Figure 4 also highlights the difference of the rainfall estimates from GPCP and PAL over the tropical Southeastern Pacific and extratropical North Pacific, but with more insights. For tropical Southeastern Pacific, there appears to be more as a “detection” issue since the GPCP and PAL data are barely correlated, exhibiting both low POD and high FAR. In contrast, the extratropical North Pacific is plagued by an overestimation problem, which results in high POD and high FAR. Although the exact reason needs to be further addressed and is outside the scope of this study, this result shows the large uncertainty of precipitation measurements over the two regions.

Figure 5 further shows the improvement of GPCP v3.2 over the prior version as a function of daily rainfall intensity. The PDFs (Figs. 5a-b) indicate that the prior version of GPCP has underestimated the occurrence of both light (<2 mm/day) and heavy rainfall (>20 mm/day), and overestimated the contributions from medium rainfall (4-16 mm/day) in terms of both rain occurrence and volume. In contrast, the PDFs of GPCP v3.2 agree very well with those of PALs, pointing to the success of this new product in accurately representing the full spectrum of rainfall over oceans. GPCP v3.2 shows better rainfall detection skills across all rain intensities (Fig. 5c), especially during heavy rainfall (note the drop of HSS for GPCP v1.3 when rain rate exceeds 8 mm/day). For those detected (i.e., "hits") events, GPCP v3.2 tends to overestimate rainfall under various intensities while GPCP v1.3 tends to largely underestimate it. The correlation decreases with increased rain rates, but the correlation value for GPCP v3.2 is consistently higher (better) than v1.3 by about 0.16.

5 Conclusions

Satellite precipitation products such as GPCP have long served as valuable sources of oceanic precipitation information, which is critical for our understanding of the climate and weather systems, global water and energy cycles, and upper ocean processes. Prior to this study, our knowledge of GPCP precipitation estimation performance over oceans was limited due to insufficient in-situ observations. With recent advances in oceanic observing technology, an increasing number of PALs have been deployed in global oceans to collect minute-scale oceanic rainfall data with a surface sampling area similar to space-borne sensors. These PALs, mostly drifting at 1-km depth along with Argo floats plus a several others on subsurface moorings, cover a broad expanse of ocean areas and many years of time, providing us with an unprecedented opportunity to validate satellite precipitation estimates over oceans. Using 58 PALS as a reference Bytheway et al. (2023) reviewed IMERG, CMORPH, and PDIR-Now, while this study evaluates the GPCP daily products, including the widely-used GPCP v1.3 and the newly released GPCP v3.2. Through a suite of evaluation metrics, we compare the two GPCP products and assess their performance as a function of time scale, region, and rainfall intensity. To the best of our knowledge, this is the first study to validate GPCP daily products using a comprehensive in-situ oceanic dataset of PALs.

GPCP v1.3 and v3.2 perform similarly at multi-year scale. Their multi-year mean rainfall estimates are highly correlated with PAL observations (CC of ∼0.9) with only slight underestimation (7.8 % for v1.3 and 3.9% for v3.2). This demonstrates their reasonable performance in characterizing rainfall climatology over oceans and a slight improvement at multi-year time scales from v3.2. The two versions also capture well the seasonality and intra-annual variations of rainfall over most oceans (e.g., the tropical Northeastern Pacific, tropical Northwestern Pacific, subtropical North Atlantic, and tropical North Indian Ocean) with comparable performance.

When evaluated at daily scale, GPCP v3.2 remarkably outperforms the previous version (v1.3) in terms of rain occurrence and rain intensity. Compared to GPCP v1.3, GPCP v3.2 reduces FAR and thus improves HSS. It also consistently increases CC at most locations. The conditional analysis, which evaluates GPCP's performance as a function of rain intensity, further indicates that GPCP v3.2 consistently exhibits improved skill at different intensities. Its estimated probability distribution functions for rainfall occurrence and volume closely align with those from PALs, whereas GPCP v1.3 underestimates the occurrence of both light (<2 mm/day) and heavy rainfall (>20 mm/day) and overestimates the contributions from medium rainfall (4-16 mm/day).

Our evaluation highlights two regions, the tropical Southeastern Pacific and extratropical North Pacific, where both versions of GPCP products exhibit similar performance and show noticeable differences from PAL observations at multiple time scales. Although the precise causes require detailed analysis outside the scope of this study, the present work highlights the challenges of accurately measuring precipitation with GPCP in these two regions.

This study provides valuable insights into the performance of GPCP daily products over oceans using in-situ observations from 58 PALs across several oceanic regions. It is important to recognize that these PALs are still limited in time and spatial coverage and do not cover the entire global ocean, especially in the southern part. The deployment of additional PALs would certainly increase the opportunity to further evaluate satellite precipitation products, which is needed to understand how best to use them and how to guide their improvements.

Open Research Section

GPCP v1.3 daily data can be obtained from the NOAA National Centers for Environmental Information (NCEI) as part of NOAA Climate Data Record (CDR) Program at `https://www.ncei.noaa.gov/data/global-precipitation-climatology-project-gpcp-daily/access/`. GPCP v3.2 daily data can be accessed from the NASA Goddard Earth Sciences Data and Information Services Center (GES DISC) at `https://disc.gsfc.nasa.gov/datasets/GPCPDAY_3.2/summary`. The PAL dataset archive is currently available at `https://downloads.psl.noaa.gov/psd3/cruises/PAL/`, and will be also available at NASA ERATHDATA portal at `https://doi.org/10.5067/GPMGV/PAL/DATA101`.

Acknowledgments

ZL, EJT and HC were supported in part by the National Aeronautics and Space Administration (NASA) Precipitation Measurement Mission (PMM) through interagency NOAA/NASA agreement 80HQTR20T0049, in part by the NASA Ocean Salinity Science Team (OSST) through interagency NOAA/NASA agreement 80HQTR20T0046, and in part by the National Oceanic and Atmospheric Administration (NOAA) Joint Polar Satellite System (JPSS) Proving Ground and Risk Reduction (PGRR) Program. Funding went to the Cooperative Institute for Research in the Atmosphere (CIRA) at Colorado State University through NOAA grant NA19OAR4320073. AB was supported by NASA MEaSUREs (NNH17ZDA001N-MEASURES) program.

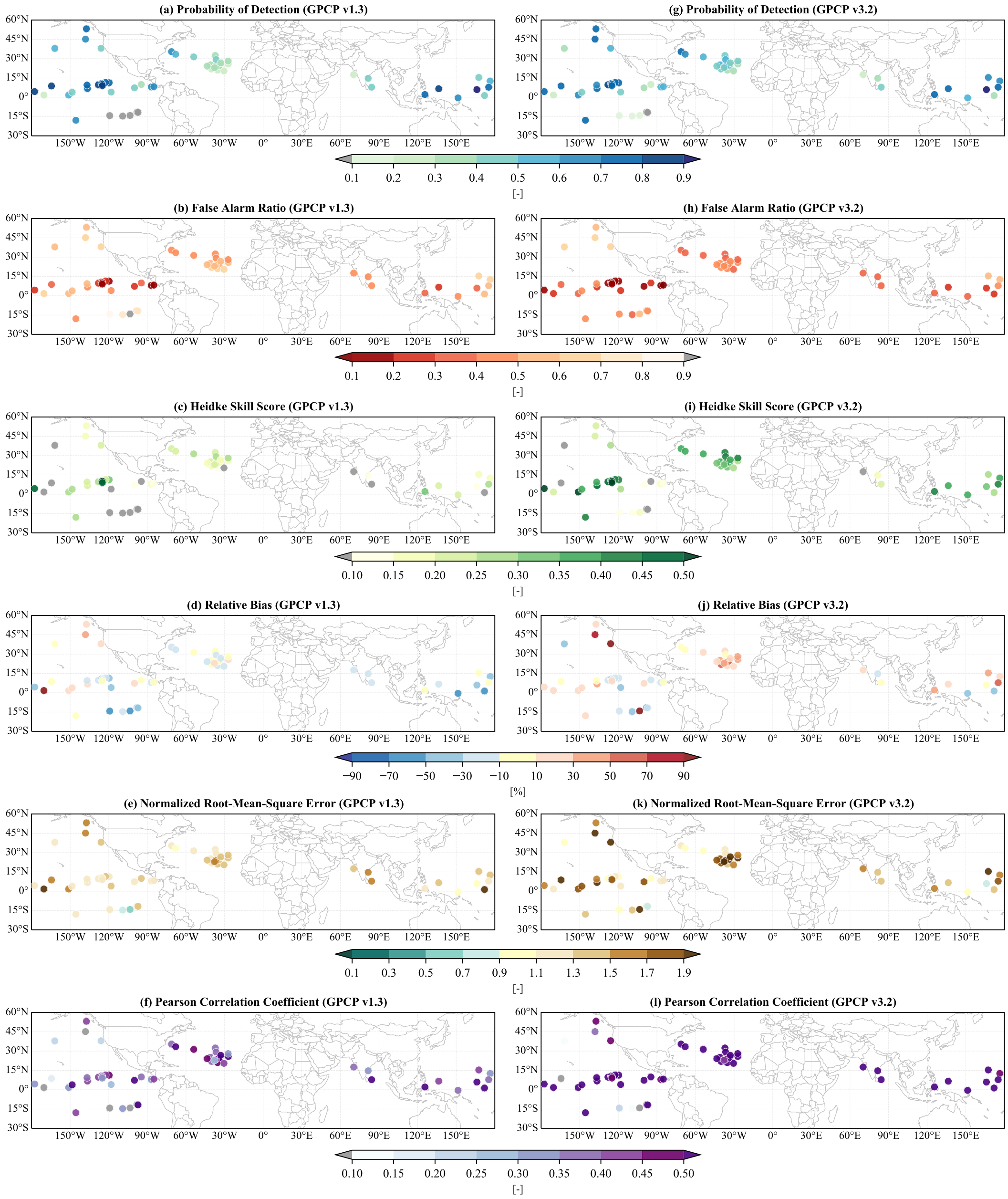

Figure 4. Spatial maps of (a, g) probability of detection (POD), (b, h) false alarm ratio (FAR), (c, i) Heidke skill score (HSS); and conditional (d, j) relative bias (RB), (e, k) normalized root-mean-square error (NRMSE), and (f, l) Pearson's correlation coefficient (CC) for daily GPCP v1.3 (left panels) and GPCP v3.2 (right panels) estimates against PALs. The circles represent the drifting end location of PALs, and rain detection threshold is 0.5 mm/day.

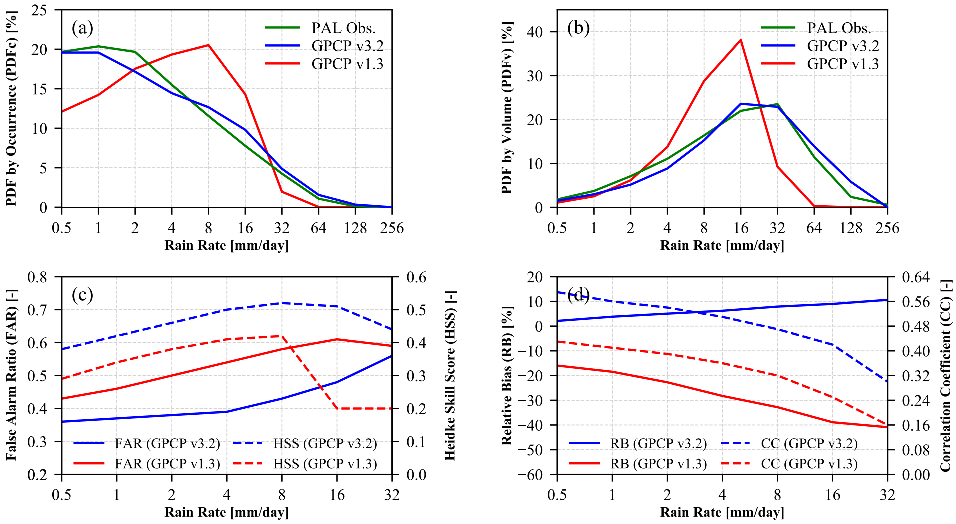

Figure 5. Comparison of (a) probability distribution function by occurrence (PDFc), (b) probability distribution function by volume (PDFv), (c) rainfall detection skills (FAR and HSS), and (d) estimation metrics (RB and CC) as a function of daily rainfall intensity for GPCP products.

References

Adler, R. F., Gu, G., Huffman, G. J., Sapiano, M. R. P., & Wang, J.-J. (2020). GPCP and the Global Characteristics of Precipitation. In V. Levizzani, C. Kidd, D. B. Kirschbaum, C. D. Kummerow, K. Nakamura, & F. J. Turk (Eds.), *Satellite Precipitation Measurement: Volume 2* (pp. 677–697). Springer International Publishing. doi: 10.1007/978-3-030-35798-6_11

Adler, R. F., Huffman, G. J., Chang, A., Ferraro, R., Xie, P.-P., Janowiak, J., … Nelkin, E. (2003). The Version-2 Global Precipitation Climatology Project (GPCP) Monthly Precipitation Analysis (1979–Present). *Journal of Hydrometeorology*, *4*(6), 1147–1167. doi: 10.1175/1525-7541(2003)004⟨1147:TVGPCP⟩2.0.CO;2

Adler, R. F., Sapiano, M., & Wang, J.-j. (2017, August). *Climate Algorithm Theoretical Basis Document (C-ATBD) for Global Precipitation Climatology Project (GPCP) Daily Analysis Precipitation –GPCP Daily CDR.*

Adler, R. F., Wang, J.-J., Gu, G., & Huffman, G. J. (2009). A Ten-Year Tropical Rainfall Climatology Based on a Composite of TRMM Products. *Journal of the Meteorological Society of Japan. Ser. II*, *87A*, 281–293. doi: 10.2151/jmsj.87A.281

Arabzadeh, A., Ehsani, M. R., Guan, B., Heflin, S., & Behrangi, A. (2020). Global Intercomparison of Atmospheric Rivers Precipitation in Remote Sensing and Reanalysis Products. *Journal of Geophysical Research: Atmospheres*, *125*(21). doi: 10.1029/2020JD033021

Arkin, P. A., & Xie, P. (1994). The Global Precipitation Climatology Project: First Algorithm Intercomparison Project. *Bulletin of the American Meteorological Society*, *75*(3), 401–419. doi: 10.1175/1520-0477(1994)075⟨0401:TGPCPF⟩2.0.CO;2

Behrangi, A., Lebsock, M., Wong, S., & Lambrigtsen, B. (2012). On the Quantification of Oceanic Rainfall Using Spaceborne Sensors. *Journal of Geophysical Research: Atmospheres*, *117*(D20). doi: 10.1029/2012JD017979

Behrangi, A., & Song, Y. (2020). A New Estimate for Oceanic Precipitation Amount and Distribution Using Complementary Precipitation Observations from Space and Comparison with GPCP. *Environmental Research Letters*, *15*(12), 124042. doi: 10.1088/1748-9326/abc6d1

Bolvin, D. T., Huffman, G. J., Nelkin, E. J., & Tan, J. (2021). Comparison of Monthly IMERG Precipitation Estimates with PACRAIN Atoll Observations. *Journal of Hydrometeorology*. doi: 10.1175/JHM-D-20-0202.1

Bowman, K. P. (2005). Comparison of TRMM Precipitation Retrievals with Rain Gauge Data from Ocean Buoys. *Journal of Climate*, *18*(1), 178–190. doi: 10.1175/JCLI3259.1

Bytheway, J. L., Thompson, E. J., Yang, J., & Chen, H. (2023). Evaluating Satellite Precipitation Estimates Over Oceans Using Passive Aquatic Listeners. *Geophysical Research Letters*, *50*(6), e2022GL102087. doi: https://doi.org/10.1029/2022GL102087

Durack, P. (2015). Ocean Salinity and the Global Water Cycle. *Oceanography*, *28*(1), 20–31. doi: 10.5670/oceanog.2015.03

Hartmann, D. L. (2016). Chapter 5 - The Hydrologic Cycle. In D. L. Hartmann (Ed.), *Global Physical Climatology (Second Edition)* (Second Edition ed., p. 131-157). Boston: Elsevier. doi: https://doi.org/10.1016/B978-0-12-328531-7.00005-0

Huffman, G. J. (1997). Estimates of Root-Mean-Square Random Error for Finite Samples of Estimated Precipitation. *Journal of Applied Meteorology*, *36*(9), 1191–1201. doi: 10.1175/1520-0450(1997)036⟨1191:EORMSR⟩2.0.CO;2

Huffman, G. J., Adler, R. F., Arkin, P., Chang, A., Ferraro, R., Gruber, A., … Schneider, U. (1997). The Global Precipitation Climatology Project (GPCP)

Combined Precipitation Dataset. *Bulletin of the American Meteorological Society*, *78*(1), 5–20. doi: 10.1175/1520-0477(1997)078⟨0005:TGPCPG⟩2.0.CO;2

Huffman, G. J., Adler, R. F., Morrissey, M. M., Bolvin, D. T., Curtis, S., Joyce, R., … Susskind, J. (2001). Global Precipitation at One-Degree Daily Resolution from Multisatellite Observations. *Journal of Hydrometeorology*, *2*(1), 36–50. doi: 10.1175/1525-7541(2001)002⟨0036:GPAODD⟩2.0.CO;2

Huffman, G. J., Alder, R. F., Behrangi, A., Bolvin, D. T., Nelkin, E. J., & Ehsani, M. R. (2023a, January). *Algorithm Theoretical Basis Document (ATBD) for, Global Precipitation Climatology Project Version 3.2 Daily Precipitation Data.*

Huffman, G. J., Alder, R. F., Behrangi, A., Bolvin, D. T., Nelkin, E. J., & Ehsani, M. R. (2023b, January). *Algorithm Theoretical Basis Document (ATBD) for, Global Precipitation Climatology Project Version 3.2 Monthly Precipitation Data.*

Huffman, G. J., Bolvin, D. T., Braithwaite, D., Hsu, K., Joyce, R., Kidd, C., … Xie, P. (2019, March). *Algorithm Theoretical Basis Document (ATBD) Version 06, NASA Global Precipitation Measurement (GPM) Integrated Multi-satellitE Retrievals for GPM (IMERG).*

Kidd, C., Becker, A., Huffman, G. J., Muller, C. L., Joe, P., Skofronick-Jackson, G., & Kirschbaum, D. B. (2017). So, How Much of the Earth's Surface Is Covered by Rain Gauges? *Bulletin of the American Meteorological Society*, *98*(1), 69–78. doi: 10.1175/BAMS-D-14-00283.1

Kidd, C., Huffman, G., Maggioni, V., Chambon, P., & Oki, R. (2021). The Global Satellite Precipitation Constellation: Current Status and Future Requirements. *Bulletin of the American Meteorological Society*, *102*(10), E1844–E1861. doi: 10.1175/BAMS-D-20-0299.1

Klepp, C., Michel, S., Protat, A., Burdanowitz, J., Albern, N., Kähnert, M., … Buehler, S. A. (2018). Oceanrain, A New In-situ Shipboard Global Ocean Surface-reference Dataset of All Water Cycle Components. *Scientific Data*, *5*(1), 1–22.

Lagerloef, G., Schmitt, R., Schanze, J., & Kao, H.-Y. (2010). The Ocean and the Global Water Cycle. *Oceanography*, *23*(4), 82–93. doi: 10.5670/oceanog.2010.07

Lebedev, K., Yoshinari, H., Maximenko, N., & Hacker, P. (2007). *YoMaHa'07: Velocity Data Assessed from Trajectories of Argo Floats at Parking Level and at the Sea Surface* (Tech. Rep. No. 4(2)). IPRC Technical Note.

Levizzani, V., Kidd, C., Aonashi, K., Bennartz, R., Ferraro, R. R., Huffman, G. J., … Wang, N. (2018). The Activities of the International Precipitation Working Group. *Quarterly Journal of the Royal Meteorological Society*, *144*(S1), 3–15. doi: 10.1002/qj.3214

Li, Z., Yang, D., & Hong, Y. (2013). Multi-scale Evaluation of High-resolution Multi-sensor Blended Global Precipitation Products over the Yangtze River. *Journal of Hydrology*, *500*, 157–169. doi: 10.1016/j.jhydrol.2013.07.023

Lindstrom, E., Bryan, F., & Schmitt, R. (2015). SPURS: Salinity Processes in the Upper-ocean Regional Study. *Oceanography*, *28*(1), 14–19.

Lindstrom, E. J., Edson, J. B., Schanze, J. J., & Shcherbina, A. Y. (2019). SPURS-2: Salinity Processes in the Upper-Ocean Regional Study 2 – The Eastern Equatorial Pacific Experiment. *Oceanography*, 6. doi: https://doi.org/10.5670/oceanog.2019.207

Ma, B. B. (2022). Rainfall at Sea: Using the Underwater Sounds of Raindrops as a Rain Gauge for Weather and Climate. *Acoustics Today*, *18*(2), 62. doi: 10.1121/AT.2022.18.2.62

Ma, B. B., & Nystuen, J. A. (2005). Passive Acoustic Detection and Measurement of Rainfall at Sea. *Journal of Atmospheric and Oceanic Technology*, *22*.

Masunaga, H., Schröder, M., Furuzawa, F. A., Kummerow, C., Rustemeier, E., & Schneider, U. (2019). Inter-product Biases in Global Precipitation Extremes. *Environmental Research Letters*, *14*(12), 125016. doi: 10.1088/1748-9326/ab5da9

Moum, J., & Smyth, W. (2019). Upper Ocean Mixing. In *Encyclopedia of Ocean Sciences* (pp. 71–79). Elsevier. doi: 10.1016/B978-0-12-409548-9.11573-8

Nystuen, J., Riser, S., Wen, T., & Swift, D. (2011). Interpreted Acoustic Ocean Observations from Argo Floats. *The Journal of the Acoustical Society of America*, *129*(4), 2400–2400. doi: 10.1121/1.3587814

Nystuen, J. A., Anagnostou, M. N., Anagnostou, E. N., & Papadopoulos, A. (2015). Monitoring Greek Seas Using Passive Underwater Acoustics. *Journal of Atmospheric and Oceanic Technology*, *32*(2), 334–349. doi: 10.1175/JTECH-D-13-00264.1

O'Kane, T. J., Monselesan, D. P., & Maes, C. (2016). On the Stability and Spatiotemporal Variance Distribution of Salinity in the Upper Ocean. *Journal of Geophysical Research: Oceans*, *121*(6), 4128–4148. doi: 10.1002/2015JC011523

Ollitrault, M., & Colin de Verdière, A. (2014). The Ocean General Circulation near 1000-m Depth. *Journal of Physical Oceanography*, *44*(1), 384–409. doi: 10.1175/JPO-D-13-030.1

Pfeifroth, U., Mueller, R., & Ahrens, B. (2013). Evaluation of Satellite-Based and Reanalysis Precipitation Data in the Tropical Pacific. *Journal of Applied Meteorology and Climatology*, *52*(3), 634–644. doi: 10.1175/JAMC-D-12-049.1

Riser, S., Yang, J., & Drucker, R. (2019). Observations of Large-Scale Rainfall, Wind, and Sea Surface Salinity Variability in the Eastern Tropical Pacific. *Oceanography*, *32*(2), 42–49. doi: 10.5670/oceanog.2019.211

Roemmich, D., Alford, M. H., Claustre, H., Johnson, K., King, B., Moum, J., … Yasuda, I. (2019). On the Future of Argo: A Global, Full-Depth, Multi-Disciplinary Array. *Frontiers in Marine Science*, *6*, 439. doi: 10.3389/fmars.2019.00439

Rutledge, S., Chandrasekar, V., Fuchs, B., George, J., Junyent, F., Kennedy, P., & Dolan, B. (2019). Deployment of the SEA-POL C-band Polarimetric Radar to SPURS-2. *Oceanography*, *32*(2), 50–57. doi: 10.5670/oceanog.2019.212

Sallée, J.-B., Pellichero, V., Akhoudas, C., Pauthenet, E., Vignes, L., Schmidtko, S., … Kuusela, M. (2021). Summertime increases in upper-ocean stratification and mixed-layer depth. *Nature*, *591*(7851), 592–598. doi: 10.1038/s41586-021-03303-x

Sapiano, M. R. P., & Arkin, P. A. (2009). An Intercomparison and Validation of High-Resolution Satellite Precipitation Estimates with 3-Hourly Gauge Data. *Journal of Hydrometeorology*, *10*(1), 149–166. doi: 10.1175/2008JHM1052.1

Schmitt, R. W. (1995). The Ocean Component of the Global Water Cycle. *Reviews of Geophysics*, *33*(S2), 1395–1409. doi: 10.1029/95RG00184

Schumacher, C., & Houze, R. A. (2003). The TRMM Precipitation Radar's View of Shallow, Isolated Rain. *Journal of Applied Meteorology*, *42*(10), 1519–1524. doi: 10.1175/1520-0450(2003)042⟨1519:TTPRVO⟩2.0.CO;2

Smith, N., Kessler, W. S., Cravatte, S., Sprintall, J., Wijffels, S., Cronin, M. F., … Brunner, S. (2019). Tropical Pacific Observing System. *Frontiers in Marine Science*, *6*, 31. doi: 10.3389/fmars.2019.00031

Susskind, J., Piraino, P., Rokke, L., Iredell, L., & Mehta, A. (1997). Characteristics of the TOVS Pathfinder Path A Dataset. *Bulletin of the American Meteorological Society*, *78*(7), 1449–1472. doi: 10.1175/1520-0477(1997)078⟨1449:COTTPP⟩2.0.CO;2

Trenberth, K. E., Smith, L., Qian, T., Dai, A., & Fasullo, J. (2007). Estimates of the Global Water Budget and Its Annual Cycle Using Observational and Model Data. *Journal of Hydrometeorology*, *8*(4), 758–769. doi: 10.1175/JHM600.1

Wang, J.-J., Adler, R. F., Huffman, G. J., & Bolvin, D. (2014). An Updated TRMM

Composite Climatology of Tropical Rainfall and Its Validation. *Journal of Climate*, *27*(1), 273–284. doi: 10.1175/JCLI-D-13-00331.1

Yang, J., Nystuen, J. A., Riser, S. C., & Thorsos, E. I. (2023). Open Ocean Ambient Noise Data in the Frequency Band of 100 Hz–50 kHz from the Pacific Ocean. *JASA Express Letters*, *3*(3), 036001. doi: 10.1121/10.0017349

Yang, J., Riser, S., Nystuen, J., Asher, W., & Jessup, A. (2015). Regional Rainfall Measurements Using the Passive Aquatic Listener During the SPURS Field Campaign. *Oceanography*, *28*(1), 124–133. doi: 10.5670/oceanog.2015.10

Yu, L. (2011). A Global Relationship Between the Ocean Water Cycle and Near-surface Salinity. *Journal of Geophysical Research: Oceans*, *116*(C10). doi: https://doi.org/10.1029/2010JC006937

Yu, L. (2019). Global Air–Sea Fluxes of Heat, Fresh Water, and Momentum: Energy Budget Closure and Unanswered Questions. *Annual Review of Marine Science*, *11*(1), 227-248. doi: 10.1146/annurev-marine-010816-060704

Supporting Information for "Performance of GPCP Products Over Oceans: Evaluation Using Passive Aquatic Listeners"

Zhe Li[1], Elizabeth J. Thompson[2], Ali Behrangi[3], Haonan Chen[1], Jie Yang[4]

[1]Department of Electrical and Computer Engineering, Colorado State University, Fort Collins, CO 80523, USA

[2]NOAA Physical Sciences Laboratory, Boulder, CO 80305, USA

[3]Department of Hydrology and Atmospheric Sciences, The University of Arizona, Tucson, AZ 85721, USA

[4]Applied Physics Laboratory, University of Washington, Seattle, WA 98105, USA

Contents of this file

Additional Supporting Information (Files uploaded separately)

1. Overview of Passive Aquatic Listeners (PALs) used in this study (see the uploaded pals_info_summary.xlsx)

Corresponding author: Dr. Zhe Li, Colorado State University, Fort Collins, CO 80523, USA. (zhe.li@colostate.edu)

Table S1. Monthly evaluation statistics for GPCP v1.3 and v3.2 over different regions. Values outside and in the parentheses are the mean and interquartile range (IQR, i.e., 25% and 75% quantiles), respectively.

Region	RB [%]	RMSE [mm]	CC [-]
TNEP	−8.1 (−24.6, 5.6)[a]	92.5 (52.3, 113.1)	0.83 (0.78, 0.88)
	−17.6 (−34.1, 6.5)[b]	90.8 (51.5, 108.5)	0.80 (0.77, 0.89)
TSEP	−66.1 (−89.8, −80.0)	35.1 (24.0, 35.2)	0.01 (−0.19, 0.04)
	−63.7 (−88.5, −73.9)	37.7 (24.0, 35.8)	0.16 (−0.06, 0.17)
TNWP	17.5 (2.86, 21.2)	63.1 (32.8, 91.4)	0.75 (0.70, 0.83)
	31.5 (15.0, 56.9)	79.3 (49.5, 103.2)	0.48 (0.50, 0.84)
ETNP	106.2 (78.5, 125.2)	66.4 (45.9, 89.0)	0.52 (0.37, 0.68)
	100.9 (56.1, 158.6)	68.0 (56.2, 85.4)	0.56 (0.42, 0.65)
TNIO	−19.2 (−11.9, 6.2)	68.5 (27.3, 37.8)	0.75 (0.72, 0.76)
	−17.4 (4.2, 24.8)	68.7 (28.8, 37.1)	0.80 (0.76, 0.85)
STNA	−4.9 (−26.2, −11.3)	34.5 (60.8, 79.1)	0.72 (0.73, 0.79)
	13.0 (−23.4, −12.9)	34.4 (60.0, 77.4)	0.81 (0.79, 0.81)

a. for each ocean, the upper row is for GPCP v1.3.
b. for each ocean, the lower row is for GPCP v3.2.

Table S2. Daily evaluation statistics for GPCP v1.3 and v3.2 over different regions. Values outside and in the parentheses are the mean and interquartile range (IQR, i.e., 25% and 75% quantiles), respectively. Here, RB, RMSE, and CC are unconditional statistics that complement the conditional statistics as shown in Figure 4.

Region	RB [%]	RMSE [mm/day]	CC [-]
TNEP	−8.1 (−25.2, 1.4)[a]	11.3 (8.3, 14.0)	0.42 (0.39, 0.50)
	−16.3 (−30.6, 5.9)[b]	11.8 (9.0, 14.5)	0.61 (0.59, 0.70)
TSEP	−66.5 (−90.2, −72.5)	3.8 (2.4, 3.4)	0.1 (−0.01, 0.06)
	−63.5 (−88.7, −73.5)	3.9 (2.3, 3.4)	0.19 (0.05, 0.16)
TNWP	10.6 (−5.2, 19.2)	9.8 (5.9, 13.1)	0.48 (0.44, 0.53)
	30.7 (14.4, 56.8)	9.8 (5.3, 13.9)	0.70 (0.65, 0.77)
ETNP	104.2 (76.9, 131.7)	6.5 (5.2, 7.0)	0.29 (0.26, 0.33)
	104.6 (69.5, 161.8)	6.6 (5.7, 6.9)	0.45 (0.43, 0.49)
TNIO	−19.4 (−26.4, −11.4)	10.6 (8.9, 12.7)	0.43 (0.38, 0.47)
	−17.4 (−23.3, −12.6)	10.3 (9.0, 11.8)	0.62 (0.59, 0.64)
STNA	−5.6 (−12.3, 5.5)	5.0 (4.1, 5.0)	0.50 (0.49, 0.54)
	13.0 (5.4, 25.3)	5.2 (4.4, 5.5)	0.69 (0.66, 0.75)
	POD [-]	FAR [-]	HSS [-]
TNEP	0.65 (0.57, 0.80)	0.32 (0.19, 0.45)	0.24 (0.12, 0.29)
	0.61 (0.49, 0.77)	0.21 (0.12, 0.30)	0.36 (0.21, 0.49)
TSEP	0.15 (0.03, 0.06)	0.72 (0.59, 0.82)	0.04 (−0.03, 0.03)
	0.21 (0.10, 0.13)	0.46 (0.41, 0.54)	0.16 (0.10, 0.16)
TNWP	0.67 (0.48, 0.81)	0.48 (0.35, 0.58)	0.19 (0.15, 0.23)
	0.70 (0.65, 0.78)	0.38 (0.26, 0.49)	0.36 (0.32, 0.39)
ETNP	0.60 (0.51, 0.69)	0.62 (0.59, 0.65)	0.15 (0.13, 0.18)
	0.61 (0.51, 0.76)	0.61 (0.60, 0.62)	0.18 (0.16, 0.23)
TNIO	0.39 (0.34, 0.45)	0.45 (0.44, 0.46)	0.09 (0.07, 0.11)
	0.35 (0.30, 0.41)	0.37 (0.35, 0.37)	0.16 (0.13, 0.21)
STNA	0.37 (0.31, 0.39)	0.54 (0.49, 0.59)	0.21 (0.18, 0.25)
	0.48 (0.44, 0.51)	0.42 (0.39, 0.45)	0.36 (0.33, 0.38)

a. for each ocean, the upper row is for GPCP v1.3.
b. for each ocean, the lower row is for GPCP v3.2.